# Inhibition of KLF5–Myo9b–RhoA Pathway-Mediated Podosome Formation in Macrophages Ameliorates Abdominal Aortic Aneurysm

Dong Ma, Bin Zheng, Toru Suzuki, Ruonan Zhang, Chunyang Jiang, Disi Bai, Weina Yin, Zhan Yang, Xinhua Zhang, Lianguo Hou, Zhan H, Jin-kun Wen

From the Department of Biochemistry and Molecular Biology, The Key Laboratory of Neural and Vascular Biology, China Administration of Education, Hebei Medical University, China (D.M., B.Z., R.Z., C.J., D.B., W.Y., Z.Y., X.Z., J.L., L.H., J.W.), School of Public Health, North China University of Science and Technology, China (D.M., D.B.), Department of Cardiovascular Sciences, University of Leicester, UK (T.S.), Department of Thoracic Surgery, Tianjin Union Medicine Centre, China (C.J.). Department of Cardiovascular Medicine, Jichi Medical University, Tochigi; Graduate School of Medicine, The University of Tokyo, Tokyo, Japan (H.Z).

Correspondence to Jin-kun Wen, Department of Biochemistry and Molecular Biology, Hebei Medical University, 361 Zhongshan East Road, Shijiazhuang, 050017, China. E-mail: wjk@hebmu.edu.cn

***Rationale*:** Abdominal aortic aneurysms (AAAs) are characterized by pathological remodeling of the aortic wall. Although both increased Krüppel-like factor 5 (KLF5) expression and macrophage infiltration have been implicated in vascular remodeling, the role of KLF5 in macrophage infiltration and AAA formation remains unclear.
***Objective*:** To determine the role of KLF5 in AAA formation and macrophage infiltration into AAAs.
***Methods and Results*:** KLF5 expression was significantly increased in human AAA tissues and in two mouse models of experimental AAA. Moreover, in myeloid-specific Klf5 knockout mice (myeKlf5$^{-/-}$ mice), macrophage infiltration, medial smooth muscle cell loss, elastin degradation, and AAA formation were markedly decreased. In cell migration and time-lapse imaging analyses, the migration of murine myeKlf5$^{-/-}$ macrophages was impaired, and in luciferase reporter assays, KLF5 activated Myo9b transcription by direct binding to the Myo9b promoter. In subsequent co-immunostaining studies, Myo9b was colocalized with F-actin, cortactin, vinculin, and Tks5 in the podosomes of phorbol 12,13-dibutyrate-treated macrophages, indicating that Myo9b participates in podosome formation. Gain- and loss-of-function experiments showed that KLF5 promoted podosome formation in macrophages by upregulating Myo9b expression. Furthermore, RhoA-GTP levels increased after KLF5 knockdown in macrophages, suggesting that KLF5 lies upstream of RhoA signaling. Finally, Myo9b expression was increased in human AAA tissues, located in macrophages, and positively correlated with AAA size.
***Conclusions*:** These data are the first to indicate that KLF5-dependent regulation of Myo9b/RhoA is required for podosome formation and macrophage migration during AAA formation, warranting consideration of the KLF5–Myo9b–RhoA pathway as a therapeutic target for AAA treatment.

**Key Words:** aneurysm; KLF5; podosome; macrophage; motility; Myo9b; RhoA
.

**Non-standard Abbreviations and Acronyms**

Abdominal aortic aneurysm, AAA; vascular smooth muscle cell, VSMC; smooth muscle cell, SMC; angiotensin II, Ang II; tumor necrosis factor, TNF; computed tomography, CT; real-time polymerase chain reaction, RT-PCR; extracellular matrix, ECM; focal adhesion kinase, FAK; phosphoinositide-3 kinase, PI(3)-kinase; Krüppel-like factor 5, KLF5; phosphate-buffered saline, PBS; smooth muscle, SM; wild-type, WT; elastic Van Gieson, EVG; bone marrow-derived macrophage, BMM; gene ontology, GO; siRNA against KLF5, si-KLF5; transcription element search system, TESS; transforming growth factor-β control element, TCE; phorbol 12,13-dibutyrate, PDBu; filamentous actin, F-actin.

## Introduction

Abdominal aortic aneurysm (AAA) is a chronic inflammatory disease characterized by the remodeling of the aortic wall, and it frequently leads to high morbidity and mortality due to vascular dissection and rupture.[1] Although AAA formation is a multifactorial process involving the infiltration of macrophages, release of proinflammatory cytokines and proteases, elastin breakdown, vascular smooth muscle cell (VSMC) apoptosis, and increased collagen turnover, macrophages are essential contributors to the pathogenesis of AAAs.[2, 3] Accordingly, monocytes/macrophages are reportedly activated by chronic inflammatory states, including atherosclerosis and oxidative stress, and by angiotensin II (Ang II) and inflammatory cytokines. Subsequently, macrophages infiltrate vessel walls, release proteases such as elastase (MMP-12) and metalloproteinases, and degrade extracellular matrix components such as collagen and elastin.[4, 5] Simultaneously, infiltrating macrophages secrete inflammatory cytokines such as tumor necrosis factor (TNF)-α, interferon-γ, interleukin-1β, and interleukin-6 into the media and adventitia of aneurysmatic vessels, thereby exacerbating inflammatory responses.[6]

Macrophage infiltration into vessel walls requires highly coordinated reorganization of actin cytoskeletal structures to create membrane protrusions called podosomes.[7] Human and murine podosomes contain many of the structural components and signaling proteins that are commonly found in focal adhesions, including cortactin, Tks5, vinculin, paxillin, and talin.[8] Podosomes appear as small dots (punctate staining) with a lifespan of around 2-10 min. However, cytokine exposure promotes the accumulation of podosomes in ring-like structures called rosettes, which can last for hours, leading to sustained extracellular matrix (ECM) digestion.[9] In addition, podosomes contain several signaling proteins, including Src, focal adhesion kinase (FAK), phosphoinositide-3 kinase (PI(3)-kinase), p190RhoGAP, and Cdc42.[10] Among these, Rho regulation has been shown to be a key intermediate in podosome formation.[11] However, there is currently little understanding of the mechanism of macrophage migration in the context of podosome formation.

Myo9b is a member of the myosin class IX family and is a unique actin-based motor protein that contains a RhoGAP domain, which, like other RhoGAPs, is inhibitory to Rho signaling.[12] Myo9b was reportedly localized with dynamic F-actin at the extending cell front and was shown to regulate Rho signaling and subsequent cell polarization and migration.[12] Although Myo9b is expressed in osteoclasts and acts as a critical regulator of podosome patterning and osteoclast function,[13] relationships between Myo9b and aneurysm development remain unknown.

Krüppel-like factor 5 (KLF5) is a DNA-binding transcriptional regulator that regulates a number of cellular processes, including development, differentiation, proliferation, and apoptosis.[14] In the cardiovascular system, KLF5 is a target for Ang II signaling and is an essential regulator of cardiovascular remodeling.[14, 15] Although KLF5 is highly expressed in large and giant unruptured cerebral aneurysms,[16] its specific contribution to podosome formation and macrophage infiltration during AAA formation has not been investigated.

In the present study, we determined whether KLF5 modulates macrophage infiltration during AAA formation by regulating podosome formation.

## Methods

### Human Tissue Harvest

AAA tissue specimens were obtained in the operating room from 11 male patients undergoing elective open AAA repair. Nonaneurysmal infrarenal aortic wall tissue

specimens were also obtained from organ donors to serve as nonaneurysmal controls (n=7). Each of the surgical patients gave informed signed consent before donating tissue. All tissue specimens were taken after a protocol approved by the Human Tissue Research Committee of Hebei Medical University. One portion of each aortic wall specimen was fixed overnight in 10% neutral buffered formalin and processed for routine embedding in paraffin. An adjacent portion was snap-frozen in liquid nitrogen, stored at -80℃, and subsequently used for protein and nucleic acid extraction.

**Animal Experiments and Lesion Characterization**

All male mice were housed and handled according to the guidelines of the local Animal Care and Use Committee at Hebei Medical University. Myeloid-specific Klf5 knockout mice (myeKlf5$^{-/-}$ mice) were derived from breedings of floxed Klf5 mice, generously provided by Dr Huajing Wan,[17] with heterozygous LysM-cre mice (Jackson Laboratory, Bar Harbor, ME, USA). Genotyping was performed by PCR. To induce abdominal aortic aneurysms, we performed two mouse models of AngII-induced[18] and $CaPO_4$-induced AAA as previously described,[19] and as detailed in the online-only Data Supplement Methods.

**Histology**

Mice were anesthetized, euthanized, and perfused before the collection of aortas as described in the online-only Data Supplement Methods, which also contains a detailed description of cell and tissue staining and visualization procedures.

**Cell Culture**

Bone marrow–derived macrophages (BMMs) and mouse vascular smooth muscle cells (SMC), 293A cells, and mouse RAW 264.7 cells were cultured and in vitro $CaPO_4$ Treatment of SMC as detailed in the online-only Data Supplement Methods.

**Adenovirus Expression Vector and Plasmid Constructs**

The expression plasmids of KLF5 were created by the placement of mouse KLF5 cDNAs into the pEGFP-C2 vector. The 5' regulatory region of mouse Myo9b (-2000 to +1 bp) was amplified by PCR and cloned into the pGL3-Basic vector (Promega) in order to generate the Myo9b promoter-reporter pGL3-Myo9b-luc. Truncated Myo9b luciferase reporters were generated by cloning the -1164, -1059, -547, -382 and 287 to +1 regions of the Myo9b promoter into pGL3. Adenoviruses encoding Klf5 (Ad-Klf5) and control (Ad-null) were entrusted to Invitrogen.

**Small Interfering RNA Transfection**

Small interfering RNAs (si-RNAs) targeting mouse Klf5 (si-Klf5) and Myo9b (si-Myo9b) were designed and synthesized by GenePharma (Shanghai, China). Non-specific siRNA (si-NS) was purchased from Santa Cruz Biotechnology. Transfection was performed using Lipofectamine reagent (Invitrogen) following the manufacturer's instructions. Twenty-hours following transfection, mouse RAW 264.7 cells were treated with TNF-α (10 ng/mL). Cells were then harvested and lysed for western blotting.

**Luciferase Assay for Myo9b Promoter Activity**

Human embryonic kidney 293A cells were maintained as previously described.[20] $3\times10^4$ cells were seeded into each well of a 24-well plate and grown for 24 h prior to transfection with reporter plasmids and the control pTK-RL plasmid. Cells were transfected using Lipofectamine 2000 reagent (Invitrogen) according to the manufacturer's instructions. Luciferase assays were performed after 24 h using a dual luciferase assay kit (Promega).

Specific promoter activity was expressed as the relative ratio of firefly luciferase activity to Renilla luciferase activity. All promoter constructs were evaluated in a minimum of three separate wells per experiment.

**Cell Immunofluorescence, Isolation of RNA and Quantitative Real Time PCR, Western Blot Analysis, Oligonucleotide Pull-down Assay and Determination of the Amounts of Active Rho, Cdc42, and Rac Proteins**

Assessment of macrophage morphology, expression level of mRNA and protein and Determination of the Amounts of Active Rho, Cdc42, and Rac Proteins are detailed in the Methods in the online-only Data Supplement.

**Proximity Ligation Assay**

The WT and myeKlf5$^{-/-}$ macrophages were grown on cell culture inserts and incubated with 4% paraformaldehyde for 10 min. Proximity ligation assay was performed using the Rabbit PLUS and Mouse MINUS Duolink in situ proximity ligation assay (PLA) kits with Anti-Myo9b (mouse) and anti-cortactin (rabbit) (OLINK Bioscience, Uppsala, Sweden) according to the manufacturer's protocol. Subsequently, slides were dehydrated, air-dried, and embedded in DAPI-containing mounting medium. Fluorescence was detected using a confocal microscopy (DM6000 CFS, Leica).

**Migration and Invasion Assays, Scanning Electron Microscopy and Time-Lapse Experiments**

Assessment of macrophage motility is detailed in the Methods in the online-only Data Supplement.

**Analysis of Microarray Data**

For microarray analysis, total RNA was extracted by using TRIzol® extraction method and a NucleoSpin RNA II kit (Macherey Nagel, Duren, Germany), from WT (n=3) and myeKlf5$^{-/-}$ (n=3) mouse aortas at day 14. Total RNA from each sample was quantified by the NanoDrop ND-1000 and RNA integrity was assessed by standard denaturing agarose gel electrophoresis. Total RNA of each sample was used for labeling and array hybridization as the following steps: 1) Reverse transcription with by Invitrogen Superscript ds-cDNA synthesis kit; 2) ds-cDNA labeling with NimbleGen one-color DNA labeling kit; 3) Array hybridization using the NimbleGen Hybridization System and followed by washing with the NimbleGen wash buffer kit; 4) the arrays were scanned by the Agilent Scanner G2505C (KangChen Bio-tech, Shanghai P.R. China).

Expression data were normalized through the Robust Multichip Average (RMA) algorithm included in the NimbleScan software. All gene level files were imported into Agilent GeneSpring GX software (version 12.1) for further analysis. Genes in 6 samples have values greater than or equal to lower cut-off: 100.0 ("All Targets Value") were chosen for data analysis. Differentially expressed genes with statistical significance were identified through Volcano Plot filtering. GO Analysis was applied to determine the roles of these differentially expressed genes played in these biological GO terms.

**Statistical Analysis of Experimental Data**

Statistical analysis was performed using GraphPad Prism 5 software (GraphPad Software, La Jolla, CA). Two-group comparisons were analyzed by the Welch Student t test to account for unequal variances (except for higher-powered data sets with equivalent variance, where we opted for an unpaired t test). Two-sided P values of $<0.05$ were considered significant and denoted with 1, 2, or 3 asterisks when lower than 0.05, 0.01, or 0.001, respectively.

Figure data are presented as mean±SEM, whereas data in results are given as relative change in comparison with the WT. For multiple comparisons or repeated measurements, ANOVA or repeated ANOVA followed by Tukey's posthoc test was used. The Spearman coefficient of rank correlation was also used to measure correlation between the human AAA size and KLF5 or Myo9b mRNA expression.

## Results

### KLF5 Is Upregulated in Human and Experimental AAA

To investigate the roles of KLF5 in human aortic aneurysms, we initially determined KLF5 expression in AAA and normal aortic tissues. Demographic characteristics and representative axial computed tomography (CT) scans are presented with corresponding three-dimensional volume-rendered images in Online Table Ⅰ and Figure Ⅰ A. KLF5 mRNA expression was significantly higher ($P$ = 0.0054) in human AAAs than in normal aortic tissues, as indicated by real-time polymerase chain reaction (RT-PCR) experiments (Figure 1A and Online Table Ⅱ). Moreover, KLF5 immunostaining was markedly increased in human AAA tissues compared with in control tissues (Figure 1B). Thus, to identify cell types that specifically express KLF5, we examined macrophages, VSMCs, and KLF5 in human AAA tissue using confocal fluorescence microscopy. In these experiments, KLF5 was primarily colocalized with intramural macrophages and smooth muscle cells (SMCs; Figure 1C and Online Figure Ⅰ B) in AAA lesions. Among all MAC2-positive cells, the percentages of KLF5-positive macrophages were significantly higher in AAA than in controls (11.3% ± 6.2% vs. 2.8% ± 1.6%, $P$ < 0.01 vs. control; Figure 1D). Furthermore, the percentages of KLF5-positive SMCs were significantly higher in AAA than in controls (10.4% ± 2.6% vs. 2.3% ± 1.1%, $P$ < 0.05 vs. control; Figure 1E). These results suggest that both macrophages and VSMCs express KLF5 in human AAA.

We induced aneurysm formation in $ApoE^{-/-}$ mice by chronic infusion of AngII. Infusion of AngII for 4 weeks led to a significant increase in the aortic external diameter (1.63 ± 0.11 mm; $P$ < 0.001) and displayed an aneurysmal phenotype compared with saline-infused control (0.68 ± 0.02 mm; Online Figure Ⅱ A and Ⅱ B). In addition, hematoxylin and eosin staining showed luminal dilation, aortic dissection, intraluminal thrombus, decreased smooth muscle layers, and wall thinning in AngII-infused mouse aortas (Figure 1F).

Affected aortic tissues were harvested for RNA extraction and immunohistochemistry after the induction of the aneurysm. In these experiments, KLF5 expression was significantly increased by 3.37 ± 0.79-fold ($P$ < 0.01, n = 4) in AngII-infused aortic walls (Figure 1G). Furthermore, immunohistochemical KLF5 expression progressively increased with the aortic diameters after AngII infusion (Figure 1H). Moreover, confocal immunofluorescence staining of KLF5, MAC2, and smooth muscle (SM) α-actin demonstrated that KLF5 (red) was expressed in both macrophages and VSMCs in experimental AAAs (Figures 1I and 1J, Online Figure Ⅱ C-E). And a similar result was also obtained in $CaPO_4$-induced AAA model (Online Figure Ⅲ). These findings were consistent with those of human AAA tissues, suggesting that KLF5 may be relevant to the formation of aneurysms in humans and in the present mouse model of AAA.

### Myeloid-Specific Knockout of Klf5 Attenuates Macrophage Infiltration and Aneurysm Formation

KLF5 was upregulated in infiltrating macrophages and macrophage infiltration was markedly increased in human and experimental AAA tissues. Thus, to investigate the relationships between KLF5 expression and macrophage infiltration, myeloid-specific Klf5

knockout mice (myeKlf5$^{-/-}$ mice) were generated by crossing Klf5-flox mice with LysM-cre mice. Subsequently, experimental AAAs was induced in ApoE$^{-/-}$ (control) and ApoE$^{-/-}$myeKlf5$^{-/-}$ mice following chronic infusion of Ang II. As shown in Figure 2A-C, myeKlf5$^{-/-}$ mice (1.30 ± 0.12 mm, n=21) had a >30% reductions in the aortic external diameter compared with control (1.67 ± 0.17 mm, n=20, $p < 0.05$), and the survival rates were significantly higher in ApoE$^{-/-}$ myeKlf5$^{-/-}$ mice than in control mice (85.7% vs. 60%, $p < 0.05$). Moreover, hematoxylin and eosin staining showed that the myeloid-specific knockout of Klf5 effectively protected against medial SMC loss, as indicated by media thicknesses (Figure 2D). To further determine the role of macrophages in AAA formation, macrophage depletion was induced by injecting clodronate liposomes, and $CaPO_4$-induced mouse AAA models were developed. As shown in Online Figure Ⅴ, macrophage depletion markedly decreased infrarenal aortic expansion, with near absence of macrophage infiltration, suggesting that macrophages play an important role in AAA formation.

Correspondingly, co-immunostaining with anti-KLF5, anti-MAC2, anti-Ly6G and anti-SMA-α antibodies showed that KLF5-positive macrophages and neutrophils that had infiltrated the aortic wall were markedly fewer in myeKlf5$^{-/-}$ mice than in control mice (Figure 2E-G). A similar results was also obtained in $CaPO_4$-induced AAA model (Online Figure Ⅳ-Ⅶ).

We further examined the influence of myeloid KLF5 expression on leucopoiesis by comparing total leukocyte counts between control and myeKlf5$^{-/-}$ mice. The results showed that the number of neutrophils and monocytes in peripheral blood was unaffected by KLF5 expression, and the total number of leukocytes and subpopulations were similar between control and myeKlf5$^{-/-}$ mice (Online Table Ⅲ and Online Figure ⅧA and ⅧB). Although myeKlf5$^{-/-}$ mice show a significant reduction in the fraction of Ly6G$^{+}$ neutrophils in bone marrow and a significant increase in the fraction of SigF+ eosinophils in spleen, Ly6G$^{+}$ neutrophils, CD11b$^{+}$ monocytes and SigF$^{+}$ eosinophils were not altered by $CaPO_4$ exposure in number or (sub) population in bone marrow, peripheral blood and spleen except increase of monocytes in spleen by flow cytometry analysis (Online FigureⅧC-Ⅷ H).

To further validate whether myeKlf5$^{-/-}$ neutrophils affects aneurysm formation, we transiently depleted neutrophils in myeKlf5$^{-/-}$ and control mice by using rat anti-mouse Ly6G/Ly6C (Gr-1) monoclonal antibody, and confirmed that neutrophils were depleted by flow cytometry (designated anti-Ly6G$^{+}$myeKlf5-/- mice; Online Figure ⅨA and ⅨB). As shown in Online Figure ⅨC and ⅨD, anti-Ly6G$^{+}$myeKlf5$^{-/-}$ mice also had reduction in maximal aortic dilation compared with control mice exposed to $CaPO_4$ for 14 d (anti-Ly6G$^{+}$myeKlf5$^{-/-}$: 57.7 ± 4.6% vs. control: 87.1 ± 6.3%, $P<0.01$). Immunohistochemical staining showed that neutrophil depletion effectively protected against medial SMC loss induced by $CaPO_4$ exposure, and reduced the infiltration of neutrophils in myeKlf5$^{-/-}$ mice (Online Figure ⅨE-G). However, we only depleted neutrophils in WT mice did not protected against medial SMC loss induced by CaPO4 exposure, and did not reduced the macrophages in anti-Ly6G+ mice, suggesting that KLF5$^{+}$ neutrophils still facilitates aneurysm formation.

In addition, in the $CaPO_4$-injured aortic tissues of wild-type mice, M1-type macrophages rather than M2-type macrophages infiltrated into AAA tissues facilitating inflammation and AAA formation; but in myeKlf5$^{-/-}$ mouse models, the infiltrating M1-type macrophages were reduced, whereas the infiltrating M2-type macrophages were increased. Moreover, the expression of M1 macrophage markers, including TNF-α, MCP-1, IL-1β and iNOS, was also downregulated, with increased expression of M2 markers, including Arg-1, Mrc-1, PPARγ and Retnal (Online Figure Ⅹ).

Likewise, myeKlf5$^{-/-}$ macrophages derived from bone marrow of myeKlf5$^{-/-}$ mice exhibited the decreased expression of M1 markers, but the enforced expression of KLF5 in myeKlf5$^{-/-}$ macrophages resumed M1 marker expression induced by LPS treatment (Online Figure Ⅺ). Simultaneously, myeKlf5$^{-/-}$ macrophages showed less phagocytotic activity than WT macrophages, as shown by zymosan phagocytosis assay (Online Figure Ⅻ). Together, KLF5 deletion in macrophages affects the pro-inflammatory response of macrophages and phagocytotic function. We also further confirmed that KLF5 deletion in macrophages did not significantly affect the proliferation of macrophages that had infiltrated the aortic wall, as evidenced by double-immunofluorescence staining of $CaPO_4$-injured aortic sections with MAC2 and Ki67 (Online Figure XIII A), as well as by decreased PCNA expression (Online Figure XIII B).

**Defective *in Vitro* Migration of myeKlf5$^{-/-}$ Macrophages**

To further investigate the roles of KLF5 in macrophage migration and infiltration, we prepared bone marrow-derived macrophages (BMMs) from control and myeKlf5$^{-/-}$ mice and compared macrophage migration using cell scratch migration assays. These experiments showed the diminished migration of myeKlf5$^{-/-}$ macrophages into cell-denuded gaps compared with WT macrophages (Figures 3A and 3B). In further experiments, Boyden chamber transwell migration assays were performed with macrophages seeded in the upper chamber and Ang II-stimulated VSMCs in the lower chamber (Figure 3C), and the numbers of myeKlf5$^{-/-}$ and WT macrophages that migrated through the porous membrane were counted. These experiments showed that significantly fewer myeKlf5$^{-/-}$ macrophages than WT macrophages migrated across the membrane (Figures 3D and 3E). Accordingly, scanning electron microscopy showed that the pseudopodial projections formed by myeKlf5$^{-/-}$ macrophages when passing through membrane pores were fewer and shorter than those formed by WT macrophages (Figure 3F). Moreover, reduced KLF5 expression was confirmed in myeKlf5$^{-/-}$ macrophages on the other side of the membrane using dual immunofluorescence staining (Figure 3G).

Taken together, the present observations indicate that myeKlf5$^{-/-}$ macrophages have impaired migration. However, the movement of macrophages in both directions across membranes may lead to the aberrant positioning and migration of Klf5-deficient macrophages at rate similar to that of WT macrophages. Thus, to validate these observations, time-lapse imaging experiments were performed, and the effects of KLF5 deficiency on forward and backward movement were investigated using chemotaxis assays in culture dishes. Because MCP-1 or TNF-α has been shown to contribute to mouse models of AAA,[21, 22] macrophages were seeded in culture dishes and MCP-1 or TNF-α was added to one side of the culture dish to establish a spatial chemotactic gradient. Although WT macrophages exhibited marked time-dependent migration toward high concentrations of MCP-1 (Figures 3H and 3I), the movement of myeKlf5$^{-/-}$ macrophages was minimal (Figures 3H, 3J, and 3K). The results of TNF-α treatment were similar to those obtained with MCP-1 (Online Figure XV). Taken together, these data demonstrate that KLF5 is required for macrophage migration and infiltration during the formation of aneurysms.

**KLF5 Mediates Myo9b Expression via Direct Binding to the Transforming Growth Factor-β Control Element (TCE) Site-1 in the Myo9b Promoter**

To identify genes that are regulated by KLF5 during macrophage migration and infiltration, we performed RNA expression profiling using microarray analyses of AAA and normal abdominal aortas from control and ApoE$^{-/-}$myeKlf5$^{-/-}$ mice. The experiments showed that motility-related gene expression markedly differed between AAA and normal aortic tissues. Among identified genes, *Myo9a* (2.67-fold) and *Myo9b* (3.22-fold) were the most

downregulated in experimental AAA tissues from Ang II-treated ApoE$^{-/-}$myeKlf5$^{-/-}$ mice (Figure 4A). In subsequent gene ontology (GO) analyses, myosin filaments and complexes were the most enriched in GOs targeted by the genetic deletion of KLF5 (Figure 4B). Furthermore, the quantitative RT-PCR analyses of motility-related gene expression following *in vivo* Ang II treatments demonstrated that Myo9a, Myo9b, and Macf1 were significantly downregulated in AAA tissues from ApoE$^{-/-}$myeKlf5$^{-/-}$ mice compared with those from control mice (Figure 4C). Taken together, these data suggest that KLF5 is required for the expression of myosin genes.

To confirm that KLF5 directly regulates Myo9a and Myo9b gene expression, we generated KLF5 overexpressing and knockdown macrophages by infecting with Ad-Klf5 or transfecting with siRNA against KLF5 (si-Klf5), respectively. In these experiments (Figures 4D and 4E), the overexpression of KLF5 significantly increased basal and TNF-α-induced Myo9a and Myo9b expression at transcription and translation levels. Conversely, the knockdown of KLF5 by si-Klf5 blocked TNF-α-induced and basal Myo9a and Myo9b expression (Figures 4F and 4G). These results suggest that KLF5 plays a key role in the regulation of Myo9a and Myo9b expression regardless of TNF-α stimulation.

The two class IX mammalian myosins Myo9a and Myo9b are actin-based motorized signaling molecules that negatively regulate RhoA signaling,[23] and the impaired migration of Myo9b$^{-/-}$ peritoneal macrophages has been previously shown.[12] Thus, to investigate the molecular mechanisms by which KLF5 promotes Myo9b gene expression, we used Transcription Element Search System (TESS) string-based search (http://www.cbil.upenn.edu/tess/) programs, and identified five putative binding sites of KLF5 (CACCC or its reverse sequence GGGTG; TCE site) in the −1396 to +1 base pair (bp) region of the Myo9b promoter (Figure 4H). Subsequently, to determine whether KLF5 regulates the expression of Myo9b gene expression via interactions with the Myo9b promoter, we performed luciferase reporter assays in 293A cells using Myo9b promoter–luciferase reporter constructs containing murine Myo9b −1396 to +1 bp sequences. In these experiments, the overexpression of KLF5 concentration-dependently increased Myo9b promoter activity (Figure 4I). Subsequent truncation of the Myo9b promoter sequence from −1396 to −382 bp did not affect the activation of the promoter by KLF5. However, further deletion of −382 and −287 bp dramatically decreased the activation by KLF5 (Figure 4J), indicating that the TCE site 1 at −319 bp is critical for the KLF5-mediated transcriptional activation of Myo9b. Thus, to investigate whether KLF5 directly binds to TCE site-1 in macrophages, we conducted oligonucleotide pull-down assays using macrophage lysates and biotinylated oligonucleotide probes. As shown in Figure 4K, KLF5 bound only to the TCE site-1 of the Myo9b promoter, and mutation of the TCE site-1 abolished KLF5 binding. Furthermore, no KLF5 bands were detected when probes containing WT or mutant sites 2, 3, 4, or 5 were used. These results suggest that KLF5 activates Myo9b transcription by directly binding the TCE site-1 of the Myo9b promoter.

**KLF5 Deletion Reduces Podosome Rosette Formation in Macrophages by Downregulating Myo9b Expression**

Adhesion and migration of monocyte-derived cells are reportedly regulated by podosomes,[7] and KLF5 was required for macrophage migration in the present study (Figures 3A through 3K). Thus, to investigate the relationships between the KLF5-regulated migration of macrophages and podosome formation, BMMs were prepared from control and ApoE$^{-/-}$myeKlf5$^{-/-}$ mice and were treated with the inducer of podosome formation phorbol 12,13-dibutyrate (PDBu).[24] Subsequently, podosome formation was visualized in macrophages according to the immunohistochemical co-localization of filamentous actin (F-actin) and cortactin (Figure 5A). Although

podosomes can present as rosettes and as individual punctates,[25] we hardly observed podosome rosettes in macrophages under normal culture conditions (data not shown), but stimulation with PDBu promoted podosome rosette formation (Figure 5A). However, no rosette structures were observed in myeKlf5$^{-/-}$ macrophages regardless of the presence of PDBu. In addition, immunofluorescence staining with an anti-Myo9b antibody revealed the colocalization of Myo9b with F-actin and cortactin in podosome rosettes (Figure 5A), indicating that Myo9b participates in PDBu-induced podosome formation.

Because MCP-1 increased macrophage migration[26], we determined whether the numbers of cells carrying individual podosomes or podosome rosettes were altered in response to MCP-1, and whether the knockout of KLF5 affected MCP-1-induced podosome formation. These experiments showed significantly greater numbers of macrophages containing podosome rosettes among MCP-1-treated cells than among untreated cells. Moreover, the knockout of Klf5 significantly reduced the formation of podosome rosettes regardless of MCP-1 treatment (Figure 5B). Conversely, the numbers of macrophages with individual podosomes did not differ between control and myeKlf5$^{-/-}$ macrophages in the presence and absence of MCP-1 or TNF-α (Figure 5C, Online Figure XVIC and XVII).

To further demonstrate Myo9b localization in podosome rosettes, coimmunofluorescence staining was performed using anti-vinculin, anti-Tks5 (both podosome marker proteins),[27] and anti-Myo9b antibodies in PDBu-treated macrophages. In agreement with the above observations of Myo9b colocalization with F-actin and cortactin (Figure 5A and Online Figure XVIA), Myo9b colocalized with vinculin and Tks5 following PDBu and MCP-1 or TNF-α treatments (Figure 5D and Online Figure XVID). To confirm the interaction of Myo9b and cortactin, we performed an in situ PLA. Because a PLA signal can be detected when the proteins of interest are in close proximity, this technique enabled us to detect direct protein–protein (Myo9b and cortactin) interaction in macrophages. The interaction of Myo9b and cortactin in WT macrophages with PDBU and MCP-1 treatment was observed. The specificity of this interaction was confirmed by the absence of association between Myo9b with cortactin in myeKlf5$^{-/-}$ macrophages with same treatment (Figure 5E).

The specificity of anti-Myo9b antibody staining was confirmed by the absence of colocalization myo9a with cortactin and F-actin (Figure 5F), and defective podosome formation in myeKlf5$^{-/-}$ macrophages was rescued by the overexpression of KLF5, as indicated by the immunofluorescence staining of podosome markers (Figure 5G and Online Figure XVIE). Furthermore, whereas Myo9b immunostaining was barely detectable in myeKlf5$^{-/-}$ macrophages (Figures 5A and 5G), the enforced expression of KLF5 in myeKlf5$^{-/-}$ macrophages resulted in marked Myo9b staining (Figure 5G). Hence, KLF5-mediated Myo9b expression may be critical for the formation of podosome rosettes in MCP-1 or TNF-α-treated macrophages.

In further studies, we assessed podosome formation in abdominal aortas from mouse and human AAA using immunostaining. The staining of mouse and human AAA tissues for F-actin and cortactin showed the presence of podosome rosette structures that were remarkably similar to those observed *in vitro* (Figures 5H and 5I, Online Figure XVIF and XVIH). Moreover, no costaining of the podosome proteins cortactin and F-actin was observed in aortas from myeKlf5$^{-/-}$ littermates or human controls (Figure 5J and 5K, Online Figure XVIG and XVI I). These data suggest that podosomes form *in vivo*, their morphological characteristics are retained in tissues, and KLF5 facilitates podosome formation *in vivo* and *in vitro*.

**Macrophage-Specific Knockdown of Myo9b Reduces Podosome Formation and Migration of Macrophages Following Treatment with MCP-1**

To further investigate the roles of Myo9b in podosome formation and macrophage migration, we knocked down endogenous Myo9b by transfecting macrophages with mouse Myo9b-specific siRNA or non-specific siRNA. These experiments demonstrated the marked attenuation of Myo9b expression in si-Myo9b-transfected macrophages compared with cells transfected with si-NS following treatment with MCP-1 (Figure 6A). Moreover, PDBu-induced formation of podosome rosettes was significantly decreased in si-Myo9b-transfected cells regardless of MCP-1 stimulation (Figures 6B and 6C), suggesting that Myo9b is required for podosome formation in macrophages. Myo9b knockdown also led to significantly reduced macrophage migration compared with that in si-NS-transfected cells regardless of MCP-1 treatment (Figure 6D), again suggesting that podosome formation facilitates macrophage migration. Furthermore, we demonstrated that KLF5 overexpression promotes the formation of podosome rosettes in si-NS-transfected macrophages, and this effect was abrogated following Myo9b knockdown using siRNA (Figures 6E and 6F). In addition, knockdown of Myo9b also reduced podosome formation and migration of macrophages following treatment with TNF-α (Online Figure XVIII). Taken together, these findings suggest that KLF5 promotes podosome formation in macrophages by regulating Myo9b expression.

**RhoA-GTP Levels Increase after Knockdown or Deletion of KLF5 in Macrophages**

Because the activation of small GTPases Cdc42, Rac1, and RhoA is required for cell migration,[11] we investigated the roles of these molecules in TNF-α-induced podosome formation and cell migration. As shown in Figure 7A, the expression levels of GTP-bound Cdc42, Rac1, and RhoA were markedly increased within 15 min of TNF-α stimulation. In particular, GTP-bound RhoA expression was maximal at 30 min and subsequently decreased to basal levels by 6 h (Figure 7 A). Moreover, Myo9b expression progressively increased with decreases in active GTP-RhoA levels, suggesting a negative correlation between GTP-RhoA and Myo9b.

To confirm that KLF5-induced formation of podosomes is related to the activation of GTP-bound RhoA, Rac1, and Cdc42, we performed further experiments using KLF5-knockdown and -overexpressing macrophages. In these experiments, KLF5 overexpression clearly upregulated Myo9b and decreased GTP-bound RhoA expression, but did not affect the Rac1 and Cdc42 activation. In contrast, the knockdown of KLF5 markedly downregulated Myo9b expression and increased GTP-bound RhoA levels in macrophages (Figures 7B and 7C), indicating that KLF5-induced Myo9b negatively regulates RhoA signaling. In addition, the treatment of myeKlf5$^{-/-}$ macrophages with the RhoA specific inhibitor Rhosin (30 μM) led to increased PDBu-induced podosome formation. However, the inhibition of RhoA signaling by Rhosin also increased podosome formation in WT macrophages, albeit slightly (Figures 7D and 7E). Accordingly, Boyden chamber assays showed significant decreases in the numbers of migrated myeKlf5$^{-/-}$ macrophages following treatment with Rhosin (Figure 7E). These data suggest that KLF5 and KLF5-regulated Myo9b lie upstream of the RhoA signaling, and KLF5, Myo9b, and RhoA co-regulate macrophage podosome formation and migration.

**Myo9b Is Upregulated and Localized to Macrophages in Human AAA**

In the present study, KLF5 promoted podosome formation and macrophage infiltration by upregulating Myo9b. Thus, we performed further experiments to corroborate these data in human aortic aneurysms. Initially, we examined Myo9b expression in human AAA tissues and normal aortic tissues using confocal immunofluorescence staining for Myo9b (red) and showed markedly increased expression in human aneurysm tissues compared with normal tissues. Moreover, Myo9b localized in MAC2-positive macrophages, as indicated by the analyses of aortic tissue sections (Figure 8A). In addition, RT-PCR analyses showed significant increases in Myo9b mRNA expression in AAA samples

compared with non-aneurysm tissues (Figure 8B), further suggesting that Myo9b is induced during human AAA formation.

Finally, we investigated the correlation between Myo9b expression and AAA expansion rates in patients with initial CT diagnoses of AAAs. AAA expansion rates were calculated according to the changes in maximal anterior–posterior (AP) diameters of AAAs during the 1-year follow-up period. In the analysis, Myo9b mRNA expression in abdominal aneurysmal walls was positively correlated with AAA size. However, although a clear trend was observed, KLF5 expression was not significantly associated with AAA size, potentially reflecting more complicated functions (Figures 8C and 8D). These results suggest that Myo9b is a target of KLF5 and plays important roles in human AAA formation. Moreover, taken with the present *in vitro* and *in vivo* data, these observations suggest that Myo9b functions as an aneurysm-promoting factor during AAA formation and progression.

## Discussion

Previous studies have shown that KLF5 is highly expressed in large and giant unruptured cerebral aneurysms.[16] However, the mechanisms by which KLF5 participates in AAA formation remain unknown. Here we present *in vitro* and *in vivo* evidence of an important role of KLF5 during AAA formation. In particular, following the Ang II stimulation of abdominal aortas, KLF5 directly upregulated Myo9b expression and promoted macrophage migration by inducing the formation of podosome rosette structures and inhibiting RhoA signaling. Accordingly, (1) KLF5 knockdown attenuated macrophage migration *in vitro* and infiltration *in vivo*; (2) KLF5 directly bound the Myo9b promoter and induced myo9b expression in macrophages; (3) KLF5 promoted podosome formation and migration in macrophages, partially through Myo9b and its downstream effector RhoA; (4) KLF5 and Myo9b were co-expressed in human AAA tissues and macrophages that had infiltrated vascular walls; and (5) the upregulation of KLF5 and Myo9b expression was correlated with the progressive dilation of human AAAs.

KLF5 has been identified as an oncogenic transcription factor that is highly expressed in tumor cell lines, and it reportedly promotes cell proliferation and migration in several cancer types, including breast, bladder, and intestinal cancers.[28] In accordance, the present data show that KLF5 is substantially upregulated in human and experimental AAA tissues and is localized in SMCs and infiltrated macrophages. Although the proliferation-specific and anti-apoptotic roles of KLF5 have been demonstrated in VSMCs, the corresponding roles in macrophages during aneurysm formation remain unclear.

In a previous study, AAA formation in global KLF4 and SM-specific KLF4 knockout mice was demonstrated using an Ang II model of aneurysm formation.[29] Moreover, myeloid-specific conditional KLF6-deficient mice reportedly exhibited aortic dissection and the presence of intramural macrophages due to the reduced expression and secretion of granulocyte-macrophage colony- stimulating factor (GM-CSF).[30] Accordingly, myeloid-specific KLF5 knockout resulted in decreased aortic aneurysm formation and concomitantly reduced Myo9b expression in the present Ang II- or $CaPO_4$-induced mouse AAA models. Taken together, our results indicate that KLF5 acts as an important regulator of aneurysm formation by promoting macrophage infiltration and migration.

KLF5 was previously shown to promote the migration of basal keratinocytes by promoting the transcription of integrin-linked kinase and the consequent activation of Cdc42 and myosin light chain, which are critical for cell migration and motility.[31] In the present study, several lines of evidence have implicated Myo9b as a direct target of KLF5. Specifically, KLF5 and Myo9b were co-expressed in human AAA tissues and macrophages, and the expression of Myo9b was decreased and increased following the

knockdown and overexpression of KLF5, respectively. In addition, KLF5 directly bound the Myo9b promoter and promoted Myo9b expression in macrophages. Moreover, mutation of the KLF5-binding site in the Myo9b promoter abolished KLF5-stimulatory effects on Myo9b expression, and KLF5 and Myo9b promoted macrophage migration and podosome rosette formation.

KLF5 can be induced by Ang II or proinflammatory factors such as interleukin-1β, lipopolysaccharide, and TNF-α. Accordingly, KLF5 and Myo9b were induced following treatments with TNF-α, indicating that KLF5 and its downstream target gene Myo9b are responsive to various extracellular pro-inflammatory stimuli, including Ang II and $CaPO_4$. KLF5 has been shown to regulate target genes by interacting with nuclear factor-κB.[32] However, it remains unclear whether KLF5 and nuclear factor-κB form a transcription complex at the Myo9b gene promoter.

Cell migration and invasion require the reorganization of actin cytoskeletal structures to produce membrane protrusions such as podosomes and invadopodia.[7] The formation of podosomes is necessary for cross-tissue migration during normal human development and is central to embryogenesis and angiogenesis as well as atherosclerotic plaque formation and cancer cell metastasis.[8] Podosomes are largely found in invasive cell types, including macrophages, osteoclasts, and dendritic cells,[8] and podosome deficiency leads to the reduced immunity of monocyte-derived macrophages and the bone resorption of osteoclasts, potentially reflecting their functions in motility and matrix remodeling.[33, 34] Podosomes are also found in VSMCs and may mediate VSMC migration and contribute to intimal hyperplasia during vascular injury or atherosclerosis. Although phorbol esters and cytokines have been shown to induce podosome formation, the functional relationship of podosome formation in rosettes in human AAA and mouse experimental AAA tissues has not been previously characterized. However, the present data suggest that podosomes are critical for macrophage migration and infiltration.

The Rho family of GTPases play important roles in cell migration by regulating actin organization and microtubule dynamics, myosin activity, and cell–extracellular matrix and cell–cell interactions.[35] Myo9b modulates lamellipodial protrusions and tail retractions by suppressing RhoA in migrating immune cells[12] and contains a RhoGAP domain in its tail region. Similar to other RhoGAPs, this domain promotes the hydrolysis of Rho-bound GTP to switch Rho from the active GTP-bound conformation to the inactive GDP-bound state. Accordingly, as a motorized signaling molecule, Myo9b directly links Rho signaling with the actin cytoskeleton. Endothelial and SMC podosome rosettes have been found in tumor vasculature and in miR-143 (145) knockout mouse aortas[24, 25] and play important roles in cell migration. To our knowledge, Myo9b has not previously been shown to influence AAA formation, and the roles of podosomes in the actin-rich structures of AAA remain poorly understood. However, the present gain- and loss-of-function experiments show that KLF5 negatively regulates RhoA signaling by promoting Myo9b expression, which in turn affects macrophage migration *in vitro* and infiltration *in vivo*. Moreover, Myo9b was highly expressed in the macrophages of human AAA tissues, and its expression was positively correlated with the advanced dilation of AAAs in patients. Although RhoA mediates stress fiber formation and generates contractile forces that are required for the retraction of the trailing edge during cell migration,[33] numerous studies show that the activation of RhoA products enhances the development of actin stress fibers and impairs the migration of cancer cells.[36] Although these observations are consistent with our results, recent studies suggest tumor-suppressive roles of RhoA in human lung cancer and T cell lymphoma.[36, 37] In addition, the blockade of RhoA signaling significantly increased podosome formation in myeKlf5$^{-/-}$ macrophages, suggesting KLF5-independnet podosome formation. Indeed, Mark Schramp et al reported that ERK5 promotes Src-induced podosome formation in Src-transformed fibroblasts by limiting Rho

activation[38]. Pathways through which KLF5 modulates Rho activity, podosome formation and cellular invasion are of considerable interest. Thus, the ensuing molecular mechanisms warrant further investigation.

In summary, the present data provide direct evidence that KLF5 is an important macrophage-borne stimulator of aneurysm formation, and it mediates Myo9b gene transcription by directly binding to the Myo9b gene promoter. Under these conditions, macrophage podosome formation and cell migration are promoted following the negative regulation of RhoA signaling. Taken together, these data show that the KLF5-dependent regulation of Myo9b/RhoA is required for podosome formation and cell migration in macrophages during AAA formation and warrant consideration of the KLF5–Myo9b–RhoA pathway as a therapeutic target for AAA treatment.

## Funding Sources

This work is supported by the National Natural Science Foundation of China (No. 31671182, 31271396, 31271224 and 31301136) and the National Basic Research Program of China (No. 2012CB518601).

## Disclosures

None.

## References

1. Folsom AR, Yao L, Alonso A, Lutsey PL, Missov E, Lederle FA, Ballantyne CM, Tang W. Circulating biomarkers and abdominal aortic aneurysm incidence: The atherosclerosis risk in communities (aric) study. *Circulation*. 2015;132:578-585.
2. Shah PK. Inflammation, metalloproteinases, and increased proteolysis: An emerging pathophysiological paradigm in aortic aneurysm. *Circulation*. 1997;96:2115-2117.
3. Henderson EL, Geng YJ, Sukhova GK, Whittemore AD, Knox J, Libby P. Death of smooth muscle cells and expression of mediators of apoptosis by t lymphocytes in human abdominal aortic aneurysms. *Circulation*. 1999;99:96-104.
4. Libby P, Ridker PM, Maseri A. Inflammation and atherosclerosis. *Circulation*. 2002;105:1135-1143.
5. Curci JA, Liao S, Huffman MD, Shapiro SD, Thompson RW. Expression and localization of macrophage elastase (matrix metalloproteinase-12) in abdominal aortic aneurysms. *J Clin Invest*. 1998;102:1900-1910.
6. Jones KG, Brull DJ, Brown LC, Sian M, Greenhalgh RM, Humphries SE, Powell JT. Interleukin-6 (il-6) and the prognosis of abdominal aortic aneurysms. *Circulation*. 2001;103:2260-2265.
7. Linder S, Aepfelbacher M. Podosomes: Adhesion hot-spots of invasive cells. *Trends Cell Biol*. 2003;13:376-385.
8. Ochoa GC, Slepnev VI, Neff L, Ringstad N, Takei K, Daniell L, Kim W, Cao H, McNiven M, Baron R, De Camilli P. A functional link between dynamin and the actin cytoskeleton at podosomes. *J Cell Biol*. 2000;150:377-389.
9. Destaing O, Saltel F, Geminard JC, Jurdic P, Bard F. Podosomes display actin turnover and dynamic self-organization in osteoclasts expressing actin-green fluorescent protein. *Mol Biol Cell*. 2003;14:407-416.
10. Tatin F, Varon C, Genot E, Moreau V. A signalling cascade involving pkc, src and cdc42 regulates podosome assembly in cultured endothelial cells in response to phorbol ester. *J Cell Sci*. 2006;119:769-781.
11. Nobes CD, Hall A. Rho, rac, and cdc42 gtpases regulate the assembly of multimolecular focal complexes associated with actin stress fibers, lamellipodia, and

filopodia. *Cell*. 1995;81:53-62.
12. Hanley PJ, Xu Y, Kronlage M, Grobe K, Schon P, Song J, Sorokin L, Schwab A, Bahler M. Motorized rhogap myosin ixb (myo9b) controls cell shape and motility. *Proc Natl Acad Sci U S A*. 2010;107:12145-12150.
13. McMichael BK, Scherer KF, Franklin NC, Lee BS. The rhogap activity of myosin ixb is critical for osteoclast podosome patterning, motility, and resorptive capacity. *PLoS One*. 2014;9:e87402.
14. Suzuki T, Sawaki D, Aizawa K, Munemasa Y, Matsumura T, Ishida J, Nagai R. Kruppel-like factor 5 shows proliferation-specific roles in vascular remodeling, direct stimulation of cell growth, and inhibition of apoptosis. *J Biol Chem*. 2009;284:9549-9557.
15. He M, Han M, Zheng B, Shu YN, Wen JK. Angiotensin ii stimulates klf5 phosphorylation and its interaction with c-jun leading to suppression of p21 expression in vascular smooth muscle cells. *J Biochem*. 2009;146:683-691.
16. Nakajima N, Nagahiro S, Sano T, Satomi J, Tada Y, Yagi K, Kitazato KT, Satoh K. Kruppel-like zinc-finger transcription factor 5 (klf5) is highly expressed in large and giant unruptured cerebral aneurysms. *World Neurosurg*. 2012;78:114-121.
17. Wan H, Luo F, Wert SE, Zhang L, Xu Y, Ikegami M, Maeda Y, Bell SM, Whitsett JA. Kruppel-like factor 5 is required for perinatal lung morphogenesis and function. *Development*. 2008;135:2563-2572.
18. Daugherty A, Cassis L. Chronic angiotensin ii infusion promotes atherogenesis in low density lipoprotein receptor -/- mice. *Ann N Y Acad Sci*. 1999;892:108-118.
19. Yamanouchi D, Morgan S, Stair C, Seedial S, Lengfeld J, Kent KC, Liu B. Accelerated aneurysmal dilation associated with apoptosis and inflammation in a newly developed calcium phosphate rodent abdominal aortic aneurysm model. *J Vasc Surg*. 2012;56:455-461.
20. Li HX, Han M, Bernier M, Zheng B, Sun SG, Su M, Zhang R, Fu JR, Wen JK. Kruppel-like factor 4 promotes differentiation by transforming growth factor-beta receptor-mediated smad and p38 mapk signaling in vascular smooth muscle cells. *J Biol Chem*. 2010;285:17846-17856.
21. Moehle CW, Bhamidipati CM, Alexander MR, Mehta GS, Irvine JN, Salmon M, Upchurch GR, Jr., Kron IL, Owens GK, Ailawadi G. Bone marrow-derived mcp1 required for experimental aortic aneurysm formation and smooth muscle phenotypic modulation. *J Thorac Cardiovasc Surg*. 2011;142:1567-1574.
22. Xiong W, MacTaggart J, Knispel R, Worth J, Persidsky Y, Baxter BT. Blocking tnf-alpha attenuates aneurysm formation in a murine model. *J Immunol*. 2009;183:2741-2746.
23. Bahler M, Elfrink K, Hanley PJ, Thelen S, Xu Y. Cellular functions of class ix myosins in epithelia and immune cells. *Biochem Soc Trans*. 2011;39:1166-1168.
24. Quintavalle M, Elia L, Condorelli G, Courtneidge SA. Microrna control of podosome formation in vascular smooth muscle cells in vivo and in vitro. *J Cell Biol*. 2010;189:13-22.
25. Seano G, Chiaverina G, Gagliardi PA, di Blasio L, Puliafito A, Bouvard C, Sessa R, Tarone G, Sorokin L, Helley D, Jain RK, Serini G, Bussolino F, Primo L. Endothelial podosome rosettes regulate vascular branching in tumour angiogenesis. *Nat Cell Biol*. 2014;16:931-941, 931-938.
26. Janjanam J, Chandaka GK, Kotla S, Rao GN. Plcbeta3 mediates cortactin interaction with wave2 in mcp1-induced actin polymerization and cell migration. *Mol Biol Cell*. 2015;26:4589-4606.
27. Burger KL, Davis AL, Isom S, Mishra N, Seals DF. The podosome marker protein tks5 regulates macrophage invasive behavior. *Cytoskeleton (Hoboken)*. 2011;68:694-711.

28. Dong JT, Chen C. Essential role of klf5 transcription factor in cell proliferation and differentiation and its implications for human diseases. *Cell Mol Life Sci*. 2009;66:2691-2706.
29. Salmon M, Johnston WF, Woo A, Pope NH, Su G, Upchurch GR, Owens GK, Ailawadi G. Klf4 regulates abdominal aortic aneurysm morphology and deletion attenuates aneurysm formation. *Circulation*. 2013;128:S163-S174.
30. Son BK, Sawaki D, Tomida S, Fujita D, Aizawa K, Aoki H, Akishita M, Manabe I, Komuro I, Friedman SL, Nagai R, Suzuki T. Granulocyte macrophage colony-stimulating factor is required for aortic dissection/intramural haematoma. *Nat Commun*. 2015;6:6994.
31. Yang Y, Tetreault MP, Yermolina YA, Goldstein BG, Katz JP. Kruppel-like factor 5 controls keratinocyte migration via the integrin-linked kinase. *J Biol Chem*. 2008;283:18812-18820.
32. Aizawa K, Suzuki T, Kada N, Ishihara A, Kawai-Kowase K, Matsumura T, Sasaki K, Munemasa Y, Manabe I, Kurabayashi M, Collins T, Nagai R. Regulation of platelet-derived growth factor-a chain by kruppel-like factor 5: New pathway of cooperative activation with nuclear factor-kappab. *J Biol Chem*. 2004;279:70-76.
33. Chellaiah MA, Soga N, Swanson S, McAllister S, Alvarez U, Wang D, Dowdy SF, Hruska KA. Rho-a is critical for osteoclast podosome organization, motility, and bone resorption. *J Biol Chem*. 2000;275:11993-12002.
34. Linder S, Nelson D, Weiss M, Aepfelbacher M. Wiskott-aldrich syndrome protein regulates podosomes in primary human macrophages. *Proc Natl Acad Sci U S A*. 1999;96:9648-9653.
35. Ridley AJ. Life at the leading edge. *Cell*. 2011;145:1012-1022.
36. Kong R, Yi F, Wen P, Liu J, Chen X, Ren J, Li X, Shang Y, Nie Y, Wu K, Fan D, Zhu L, Feng W, Wu JY. Myo9b is a key player in slit/robo-mediated lung tumor suppression. *J Clin Invest*. 2015;125:4407-4420.
37. Cools J. Rhoa mutations in peripheral t cell lymphoma. *Nat Genet*. 2014;46:320-321.
38. Schramp M, Ying O, Kim TY, Martin GS. Erk5 promotes src-induced podosome formation by limiting rho activation. *J Cell Biol*. 2008;181:1195-1210.

## Novelty and Significance

**What Is Known?**

- Abdominal aortic aneurysm (AAA) is a chronic inflammatory disease characterized by the remodeling of the aortic wall.
- KLF5 is an essential regulator of cardiovascular remodeling and is highly expressed in cerebral aneurysms.
- Macrophage infiltration into vessel walls depends on podosome formation; Myo9b is involved in osteoclast podosome formation.
- Myo9b regulates Rho signaling and cell migration.

**What New Information Does This Article Contribute?**

- KLF5 is required for podosome formation, macrophage migration and infiltration in vivo and in vitro.
- KLF5 activates Myo9b transcription by direct binding to the Myo9b promoter.
- Myo9b is elevated in human AAA tissues and positively correlated with AAA size.
- KLF5-dependent regulation of Myo9b/RhoA is important for podosome formation and macrophage migration during AAA formation.

Abdominal aortic aneurysm (AAA) is a permanent dilation of abdominal aorta caused by chronic inflammation, elastin breakdown and SMC apoptosis. The increasing prevalence of AAA and the lack of effective drug treatments stress the need for a detailed understanding of the disease mechanism. Inflammation has been embraced as a potential target for intervention. In particular, the accumulation and subsequent activation of leukocyte subsets, including macrophage, in aneurysmal wall have been investigated for their roles in aneurysm formation and progression in human AAA and experimental AAA. Our work demonstrates that KLF5 and Myo9b expressions are elevated in macrophages that had infiltrated the aneurysmal tissues. In the AngII- and $CaPO_4$-induced mouse AAA model, deletion of the KLF5 in macrophages protects mice from AAA formation and aneurysm-associated pathological changes, including SMC depletion, macrophage infiltration and inflammation. In cultured macrophages, we found that KLF5 is required for both MCP-1- and TNF-α-induced infiltration and Myo9b–mediated inhibition of RhoA signaling and podosome formation. We show that Myo9b acts as a downstream regulator of KLF5 in macrophages. Our data suggest that KLF5-dependent regulation of Myo9b/RhoA is required for podosome formation and macrophage migration during AAA formation, warranting consideration of the KLF5-Myo9b-RhoA pathway as a therapeutic target for AAA treatment.

# Figure 1

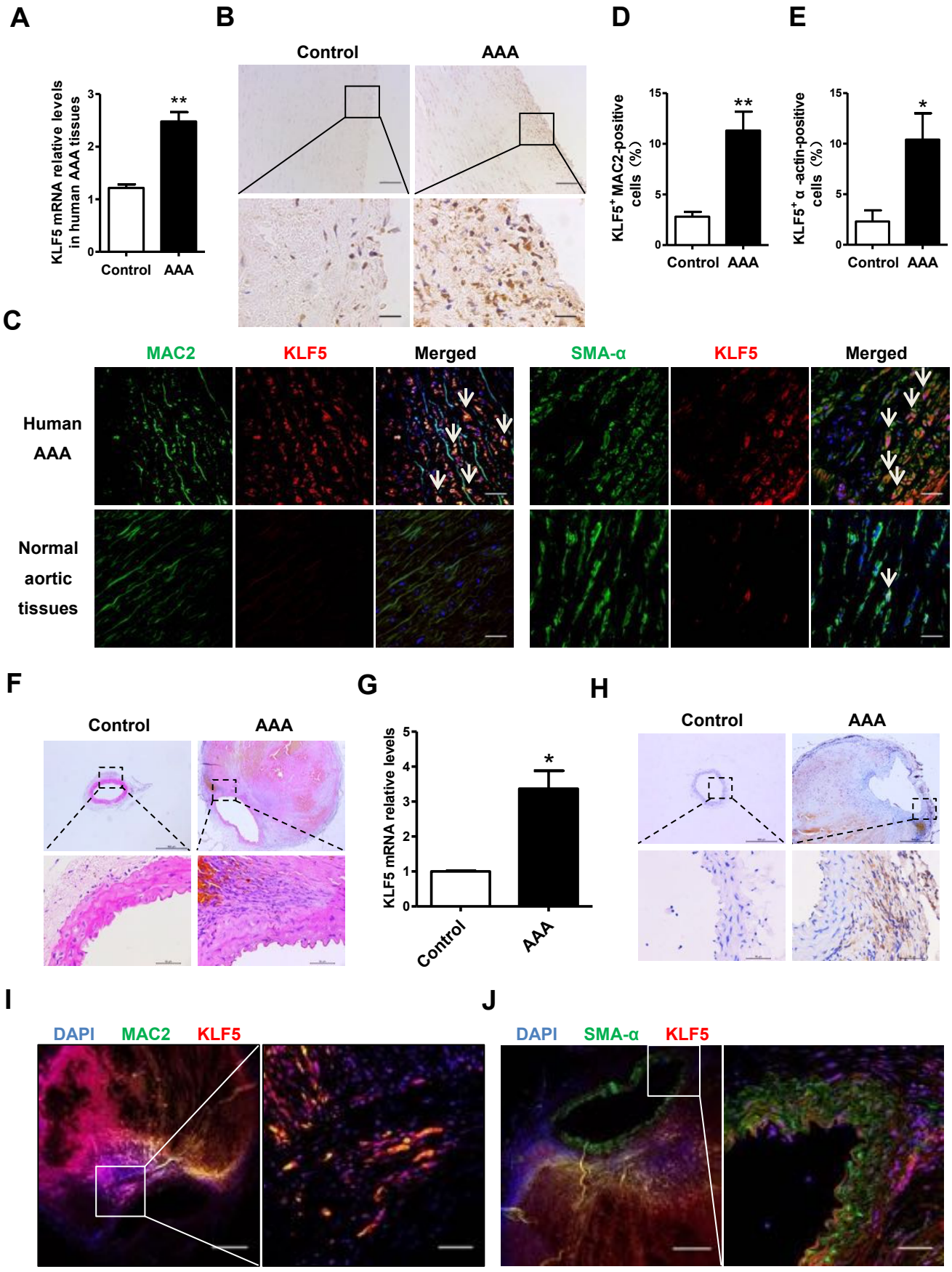
A
KLF5 mRNA relative levels in human AAA tissues
**
Control
AAA
B
Control
AAA
D
KLF5+ MAC2-positive cells (%)
**
Control
AAA
E
KLF5+ α -actin-positive cells (%)
*
Control
AAA
C
MAC2
KLF5
Merged
SMA-α
KLF5
Merged
Human AAA
Normal aortic tissues
F
Control
AAA
G
KLF5 mRNA relative levels
*
Control
AAA
H
Control
AAA
I
DAPI
MAC2
KLF5
J
DAPI
SMA-α
KLF5

**Figure 1. KLF5 is elevated in human abdominal aortic aneurysms (AAAs) and AngII-induced AAA model. A**, qRT-PCR for KLF5 expression in human AAA tissues (n=11) and normal abdominal aorta (n=7). ***P* < 0.01 vs. control. **B**, Representative photographs of immunohistochemical staining for KLF5 in AAA tissue and control. Scale bars=50 μm. **C**, Confocal immunofluorescence performed on human AAA sections stained with MAC2, SM α-actin, KLF5, and 4′,6-diamidino-2-phenylindole (DAPI). Arrows indicate $KLF5^+$ MAC2-positive or $KLF5^+$ SM α-actin-positive cells. Scale bars=50 μm. **D** and **E**, Statistics of $KLF5^+$ MAC2-positive cells and $KLF5^+$ SM α-actin-positive cells in human AAA tissue and control. **P*＜0.05 and ***P*＜0.01 vs. control. **F**, Representative photographs of hematoxylin and eosin (HE)-stained abdominal aortic sections of C57BL/6 mice infused with saline or Ang II for 28 d. **G**, KLF5 mRNA expression relative to GAPDH in the injured aortas of C57BL/6 mice infused with saline or Ang II for 28 d. Data represent the mean±SEM, **P*＜0.05 vs. saline. n=4 in each group. **H**, Representative images immunostained with KLF5 (brown) in the abdominal aortic sections of C57BL/6 mice infused with saline or Ang II for 28 d. Scale bars=50 μm. **I** and **J**, Confocal immunofluorescence performed on mouse aortic sections stained with KLF5, MAC2, SM α-actin, and DAPI. Scale bars=50 μm.

# Figure 2

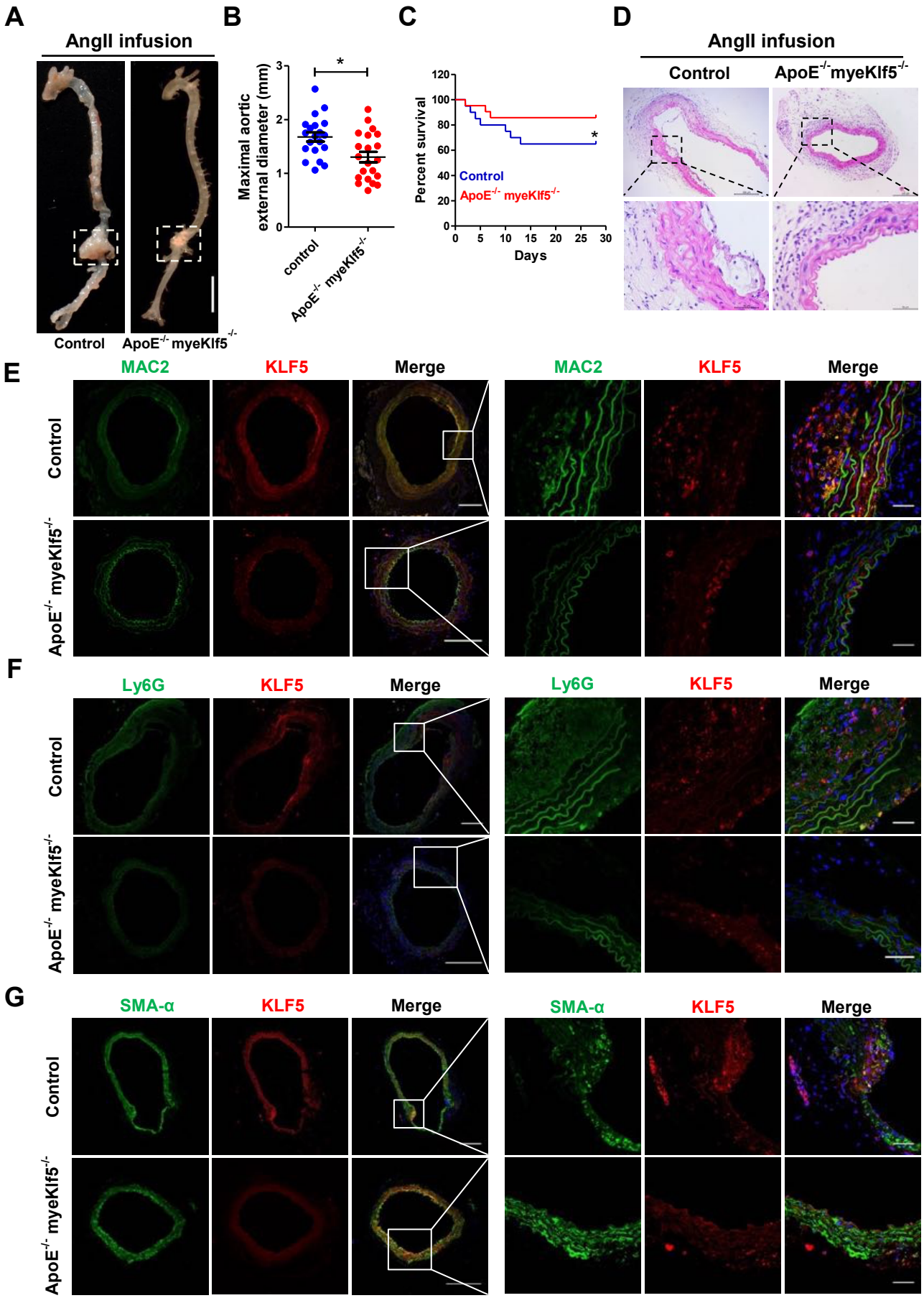
A
AngII infusion
Control
ApoE-/- myeKlf5-/-
B
Maximal aortic external diameter (mm)
control
ApoE-/- myeKlf5-/-
C
Percent survival
Control
ApoE-/- myeKlf5-/-
Days
D
AngII infusion
Control
ApoE-/-myeKlf5-/-
E
MAC2
KLF5
Merge
Control
ApoE-/- myeKlf5-/-
F
Ly6G
KLF5
Merge
Control
ApoE-/- myeKlf5-/-
G
SMA-α
KLF5
Merge
Control
ApoE-/- myeKlf5-/-

**Figure 2. Myeloid-specific knockout of Klf5 attenuates aneurysm formation. A**, Representative photographs of AAA induced by Ang II infusion (dashed). Scale bar=2.5 mm. **B**. The maximal aortic external diameter for control (n=20) and ApoE$^{-/-}$ myeKlf5$^{-/-}$ mice (n=21) exposed to Ang II for 28 d. Data represent the mean±SEM. *$P$ < 0.05 vs. control. **C**, Survival curve of Ang II-infused ApoE$^{-/-}$ (n=20) and ApoE$^{-/-}$ myeKlf5$^{-/-}$ mice (n=21). *$P$ < 0.05, log-rank test. **D**, HE-stained representative sections of aortas from the Ang II-infused control (ApoE$^{-/-}$) and ApoE$^{-/-}$ myeKlf5$^{-/-}$ mice. Scale bars=50 μm. **E** through **G**, Dual immunofluorescence staining of KLF5 (red), MAC2 (green), Ly6G (green) and SMA-α (green) in the injured aortas of control and ApoE$^{-/-}$ myeKlf5$^{-/-}$ mice exposed to Ang II for 28 d. Scale bars=50 μm.

# Figure 3

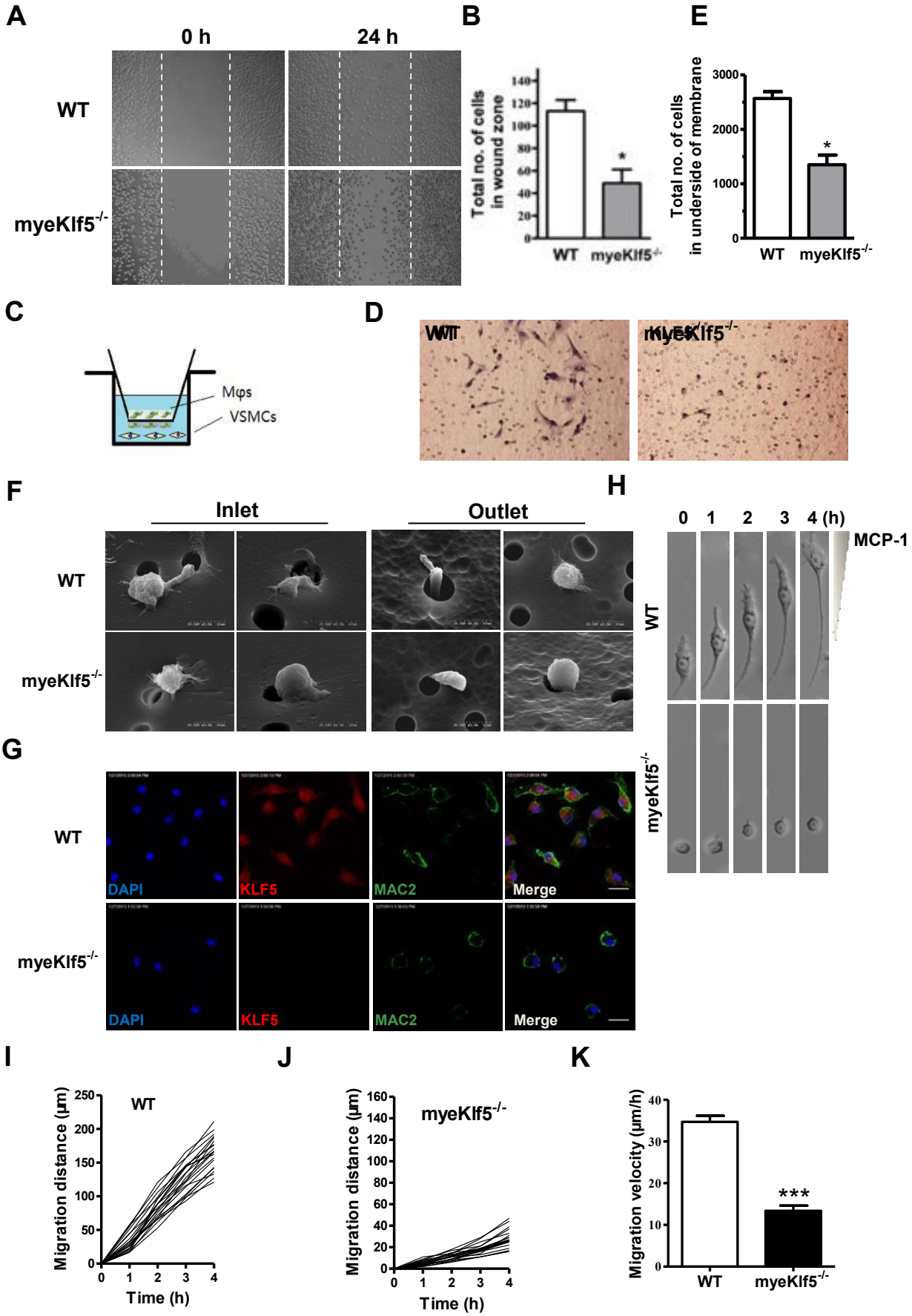
A
0 h
24 h
WT
myeKlf5-/-
B
Total no. of cells in wound zone
WT
myeKlf5-/-
E
Total no. of cells in underside of membrane
WT
myeKlf5-/-
C
Mφs
VSMCs
D
WT
myeKlf5-/-
F
Inlet
Outlet
WT
myeKlf5-/-
H
0 1 2 3 4 (h)
MCP-1
WT
myeKlf5-/-
G
WT
DAPI
KLF5
MAC2
Merge
myeKlf5-/-
DAPI
KLF5
MAC2
Merge
I
WT
Migration distance (μm)
Time (h)
J
myeKlf5-/-
Migration distance (μm)
Time (h)
K
Migration velocity (μm/h)
***
WT
myeKlf5-/-

**Figure 3. myeKlf5$^{-/-}$ macrophages are defective in their migration ability. A**, Representative photomicrographs of a scratch assay performed with macrophages from ApoE$^{-/-}$ or ApoE$^{-/-}$ myeKlf5$^{-/-}$ mice immediately after scratching and 12 h later. **B**, Quantification of cells migrating into the scratch gap. The data are mean±SEM from three independent experiments. *$P<0.05$ vs. WT. **C**, An in vitro co-culture system is shown where macrophages were seeded in the top compartment and Ang II-stimulated SMCs in the bottom compartment. **D**, Boyden chamber assay showing WT and myeKlf5$^{-/-}$ macrophages traversed the filter to the other side and stained by HE. **E**, Quantification of cells migrated to the lower side of the membrane. *$P<0.05$ vs. WT. **F**, Scanning electron microscopy showing that myeKlf5$^{-/-}$ macrophages had shorter and fewer pseudopod projections. **G**, Dual immunofluorescence staining of KLF5 (red) and MAC2 (green) in WT and myeKlf5$^{-/-}$ macrophages. Scale bars=50 μm. **H**, MCP-1-stimulated migration of WT and myeKlf5$^{-/-}$ macrophages was traced by using time-lapse imaging. **I** and **J**, Each line represents the movement of each macrophage from ApoE$^{-/-}$ and ApoE$^{-/-}$myeKlf5$^{-/-}$ mice. **K**, Migration distances per hour were measured by Image J. n=21 cells, ***$P<0.001$ vs. WT.

# Figure 4

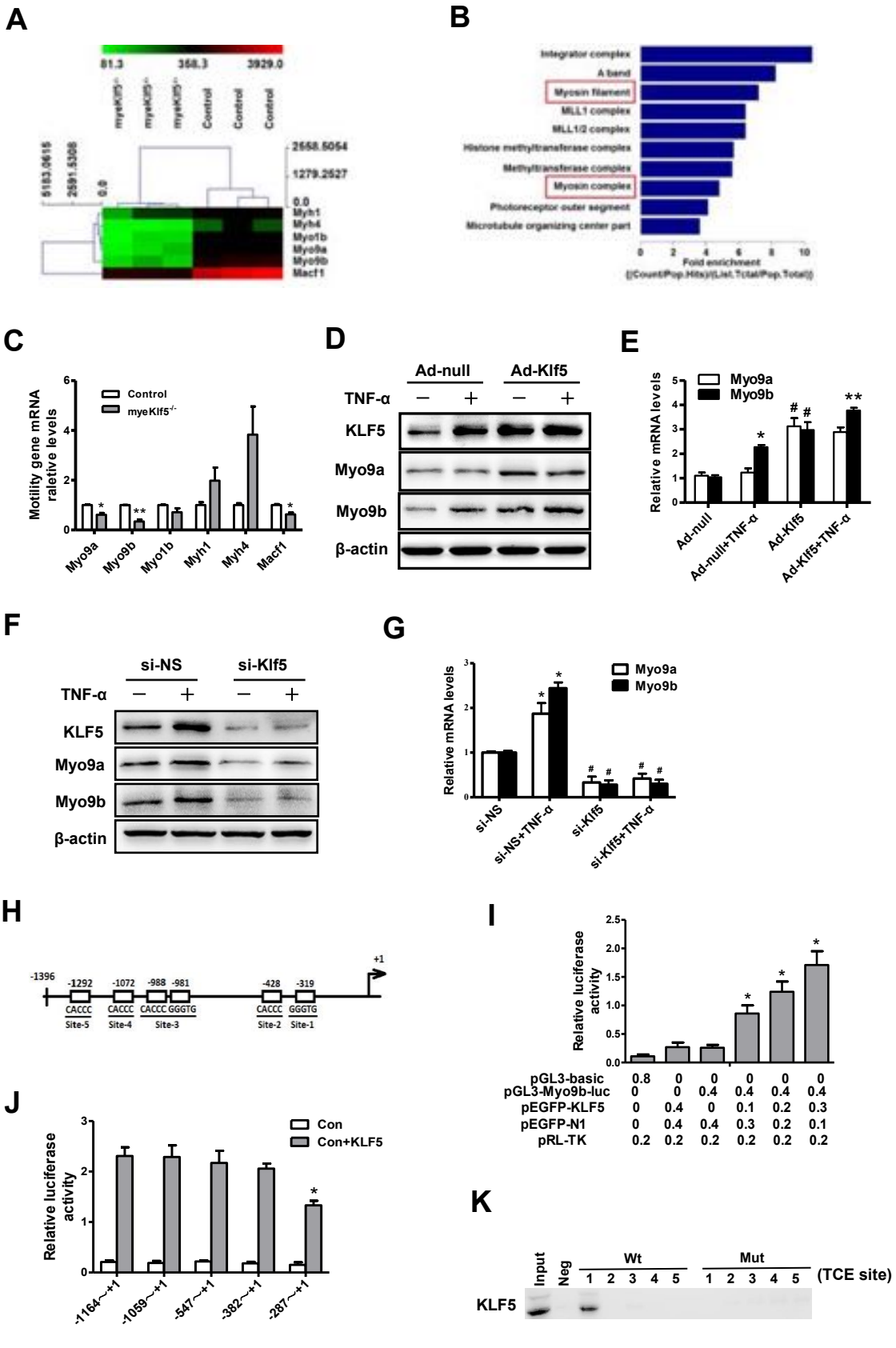
A
81.3
368.3
3929.0
mykKlf5-/-
mykKlf5-/-
mykKlf5-/-
Control
Control
Control
5183.0615
2591.5308
0.0
2558.5054
1279.2527
0.0
Myh1
Myh4
Myo1b
Myo9a
Myo9b
Macf1
B
Integrator complex
A band
Myosin filament
MLL1 complex
MLL1/2 complex
Histone methyltransferase complex
Methyltransferase complex
Myosin complex
Photoreceptor outer segment
Microtubule organizing center part
0
2
4
6
8
10
Fold enrichment
C
Motility gene mRNA raletive levels
Control
myeKlf5-/-
Myo9a
Myo9b
Myo1b
Myh1
Myh4
Macf1
D
Ad-null
Ad-Klf5
TNF-α
KLF5
Myo9a
Myo9b
β-actin
E
Relative mRNA levels
Myo9a
Myo9b
Ad-null
Ad-null+TNF-α
Ad-Klf5
Ad-Klf5+TNF-α
F
si-NS
si-Klf5
TNF-α
KLF5
Myo9a
Myo9b
β-actin
G
Relative mRNA levels
Myo9a
Myo9b
si-NS
si-NS+TNF-α
si-Klf5
si-Klf5+TNF-α
H
-1396
-1292
-1072
-988
-981
-428
-319
+1
CACCC
CACCC
CACCC GGGTG
CACCC
GGGTG
Site-5
Site-4
Site-3
Site-2
Site-1
I
Relative luciferase activity
pGL3-basic 0.8 0 0 0 0 0
pGL3-Myo9b-luc 0 0 0.4 0.4 0.4 0.4
pEGFP-KLF5 0 0.4 0 0.1 0.2 0.3
pEGFP-N1 0 0.4 0.4 0.3 0.2 0.1
pRL-TK 0.2 0.2 0.2 0.2 0.2 0.2
J
Relative luciferase activity
Con
Con+KLF5
-1164~+1
-1059~+1
-547~+1
-382~+1
-287~+1
K
Input
Neg
Wt
Mut
1 2 3 4 5
1 2 3 4 5
(TCE site)
KLF5

**Figure 4. KLF5 mediates Myo9b expression via direct binding to the TCE site-1 in the Myo9b promoter. A**, A subset of the differentially expressed mRNAs detected in the injured aortas of control ($ApoE^{-/-}$) (n=3) and myeKlf5$^{-/-}$ ($ApoE^{-/-}$ myeKlf5$^{-/-}$) mice (n=3) with microarray analysis was selected and summarized. **B**, The Gene Ontology enrichment analysis showing the significantly changed genes in the injured aortic tissues of myeKlf5$^{-/-}$ and control mice. **C**, Six changed genes were validated by qRT-PCR in the aortic tissues of control and myeKlf5$^{-/-}$ mice. *$P<0.05$ and **$P<0.01$ vs. control. **D** and **E**, Macrophages were infected with Ad-null or Ad-Klf5 for 24 h and then were treated or not with TNF-α (10 ng/mL). The expression of KLF5, Myo9a and Myo9b was analyzed by Western blotting (D) and qRT-PCR (E). *$P$<0.05 vs. Ad-null, $^{\#}P<0.05$ vs. Ad-null+TNF-α, **$P<0.05$ vs. Ad-Klf5. **F** and **G**, Macrophages were transfected with si-NS or si-Klf5 for 24 h and then treated or not with TNF-α. The expression of KLF5, Myo9a and Myo9b was examined as described above. *$P<0.05$ vs. si-NS, $^{\#}P<0.05$ vs. si-NS+TNF-α. **H**, A schematic map of the −1396 to +1 bp region of the Myo9b promoter showing the position of five KLF5-binding sites. **I**, A luciferase reporter controlled by the Myo9b promoter was transfected into 293A cells along with increasing amounts of KLF5 expression plasmid. Luciferase activity was measured using the dual luciferase reporter assay system. Data represent the relative Myo9b promoter activity normalized to pRL-TK activity. *$P < 0.05$ vs. pEGFP-N1-transfected group. **J**, 293A cells were transfected with the Myo9b promoter–reporter plasmids containing various 5'-deletion fragments. Luciferase activity was measured as described above. *$P < 0.05$ vs. promoter-reporters containing the -1164 to -382 bp region. **K**, An oligo pull-down assay was done with macrophage lysates and biotinylated double-stranded oligonucleotide containing the consensus TCE sites-1, 2, 3, 4, and 5 (Wt and Mut) as probes. The DNA-bound protein was detected by Western blotting with anti-KLF5 antibody.

# Figure 5

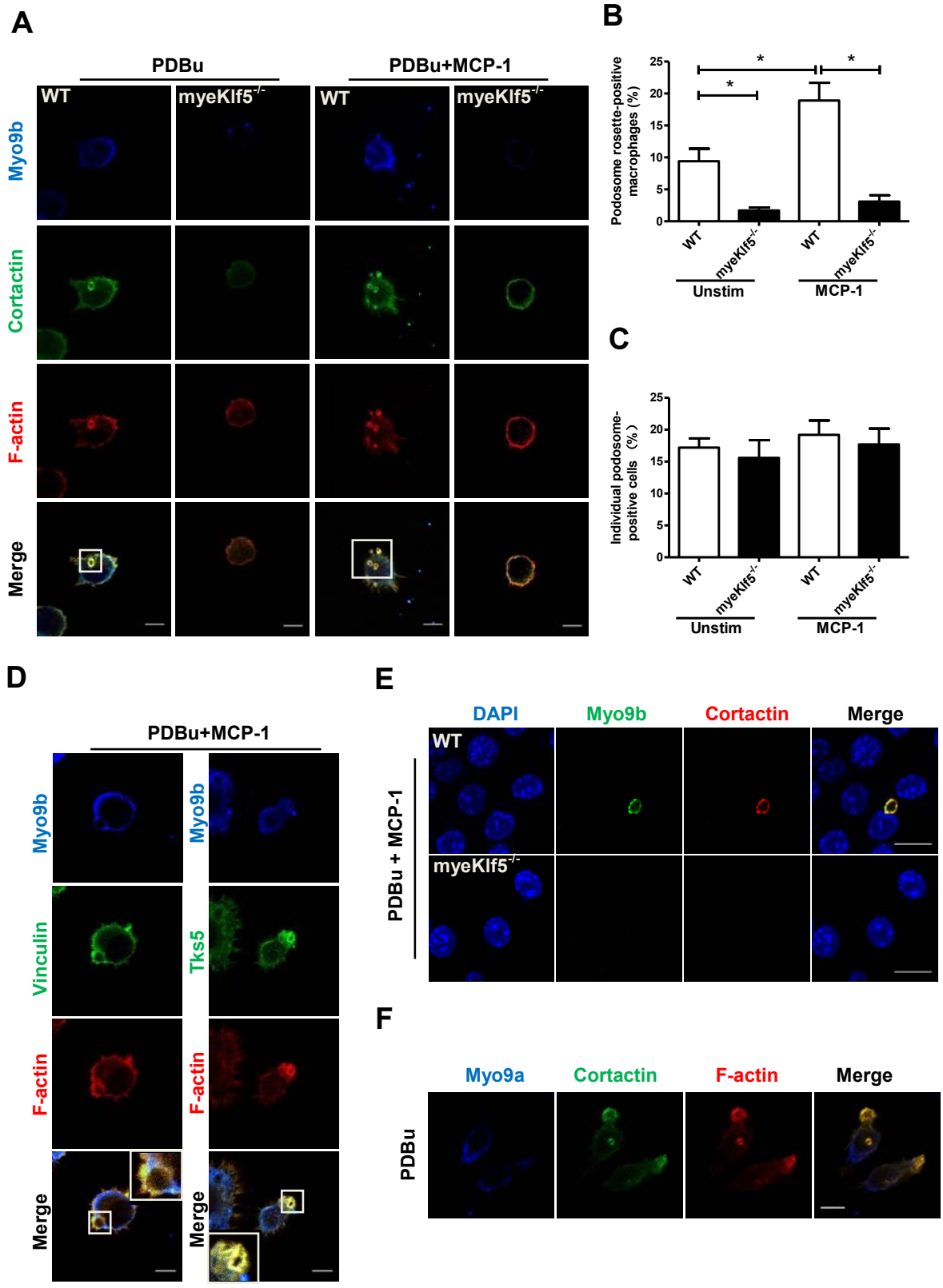
A
PDBu
PDBu+MCP-1
WT
myeKlf5-/-
Myo9b
Cortactin
F-actin
Merge
B
Podosome rosette-positive macrophages (%)
Unstim
MCP-1
C
Individual podosome-positive cells (%)
D
PDBu+MCP-1
Myo9b
Vinculin
Tks5
F-actin
Merge
E
DAPI
Myo9b
Cortactin
Merge
PDBu + MCP-1
F
Myo9a
Cortactin
F-actin
Merge
PDBu

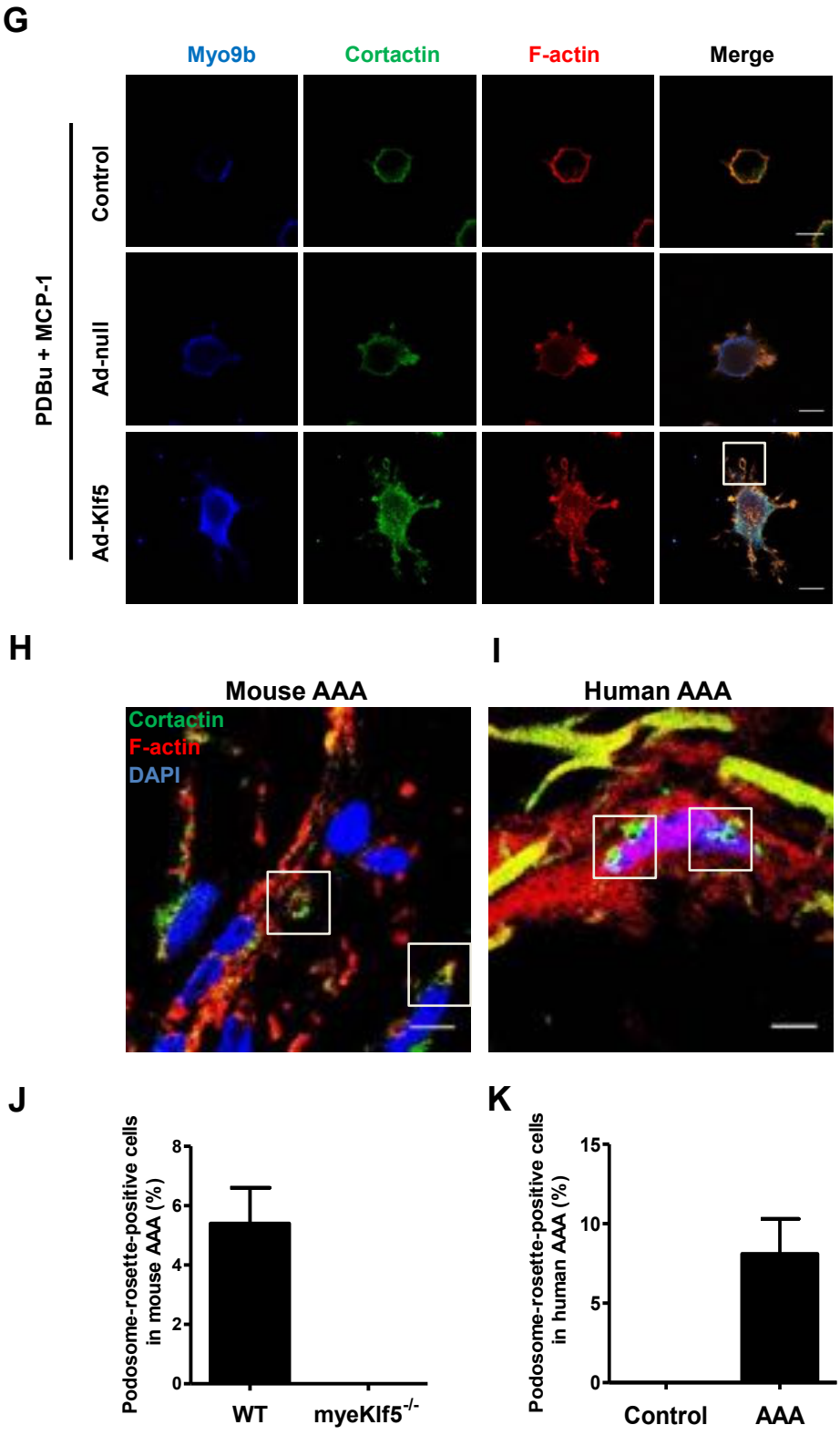
G
Myo9b
Cortactin
F-actin
Merge
PDBu + MCP-1
Control
Ad-null
Ad-Klf5
H
Mouse AAA
Cortactin
F-actin
DAPI
I
Human AAA
J
Podosome-rosette-positive cells in mouse AAA (%)
8
6
4
2
0
WT
myeKlf5-/-
K
Podosome-rosette-positive cells in human AAA (%)
15
10
5
0
Control
AAA

**Figure 5. KLF5 deletion reduces podosome rosette formation in macrophages through down-regulating Myo9b expression. A**, The WT and myeKlf5$^{-/-}$ macrophages were treated or not with MCP-1 for 24 h, and then were stimulated for 30 min with PDBu. Fluorescence staining of cortactin (anti-cortactin) and F-actin (rhodamine-phalloidin) was used to visualize podosomes. Scale bars=10 μm. **B** and **C**, The percentage of individual podosome- and podosome-rosette-positive macrophages. *$P<0.05$ vs. untreated or WT group. **D**, Colocalization of Myo9b with F-actin or vinculin and Tks5 in macrophages treated with PDBu and MCP-1. Scale bar=10 μm. **E**, Detection of Myo9b and cortactin interaction in WT and myeKlf5$^{-/-}$ macrophages using Duolink with two primary antibodies. Duolink signals are shown in red and green, DAPI was used for staining of nuclei. Stained cells were examined by confocal microscopy. Scale bars=10 μm. **F**, Colocalization of Myo9a with cortactin and F-actin was not detected. Scale bar=10 μm. **G**, myeKlf5$^{-/-}$ macrophages were infected with Ad-Klf5 or Ad-null for 24 h and then treated with MCP-1 and PDBu. Podosomes were visualized as described above. Scale bars=10 μm. **H** and **I**, Fluorescence staining of cortactin and F-actin on AAA tissue sections of the Ang II-induced WT (ApoE$^{-/-}$) mice (H) and human AAA (I). Scale bars=20 μm. **J** and **K**, The percentage of podosome-rosette-positive macrophages in AAA tissues of Ang II-induced WT (ApoE$^{-/-}$) mice and human AAA. The data represent mean±SEM of 3 independent experiments in which 400 cells were analyzed.

# Figure 6

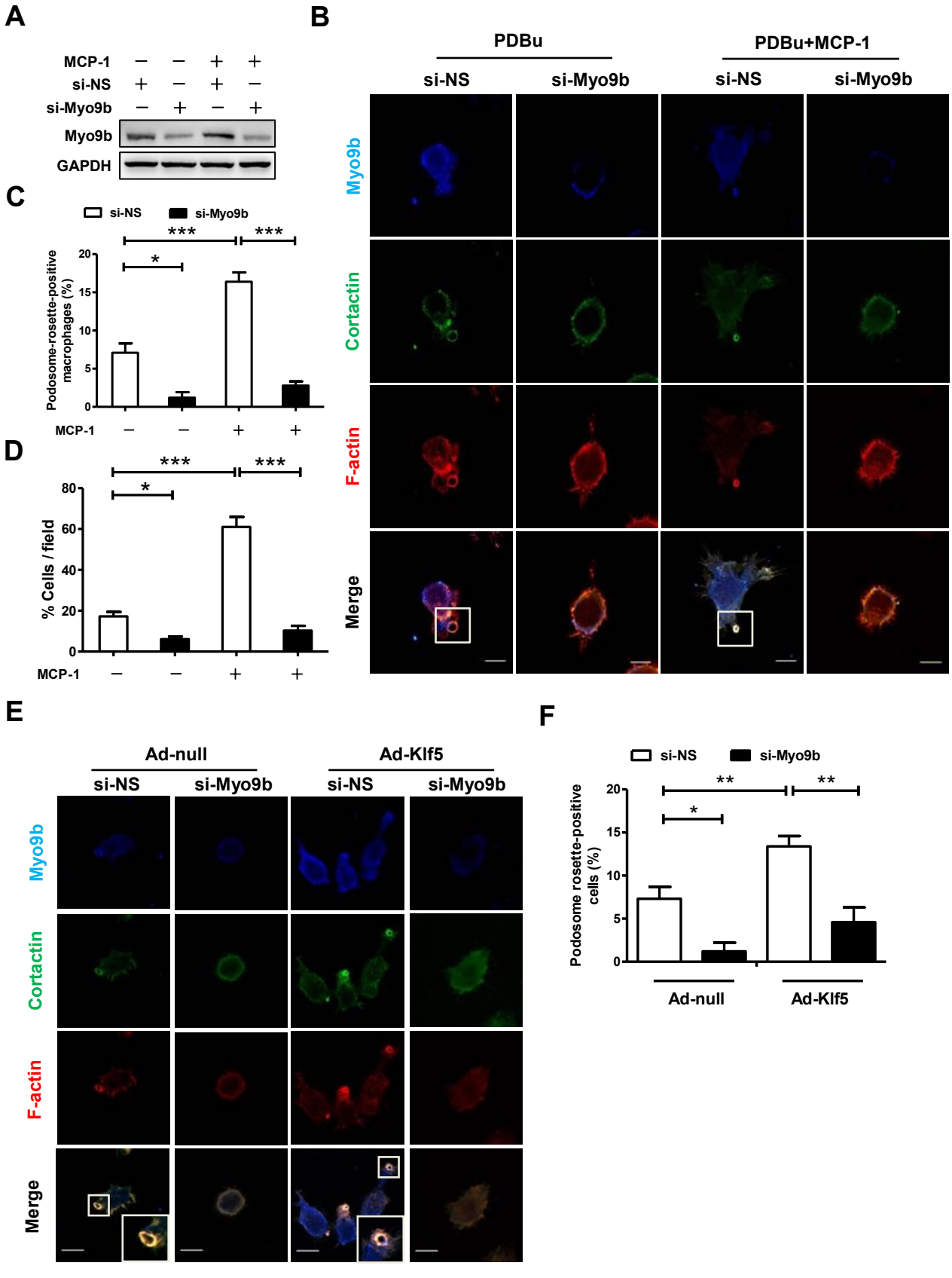
A
MCP-1
si-NS
si-Myo9b
Myo9b
GAPDH
B
PDBu
PDBu+MCP-1
si-NS
si-Myo9b
si-NS
si-Myo9b
Myo9b
Cortactin
F-actin
Merge
C
si-NS
si-Myo9b
Podosome-rosette-positive macrophages (%)
MCP-1
D
% Cells / field
MCP-1
E
Ad-null
Ad-Klf5
si-NS
si-Myo9b
si-NS
si-Myo9b
Myo9b
Cortactin
F-actin
Merge
F
si-NS
si-Myo9b
Podosome rosette-positive cells (%)
Ad-null
Ad-Klf5

**Figure 6. Myo9b knockdown reduces podosome formation and migration of macrophages induced by MCP-1. A** and **B**, Macrophages were transfected with si-Myo9b or si-NS for 24 h and then treated with MCP-1 for 24 h. Myo9b knockdown was determined by Western blotting with anti-Myo9b (A), podosomes were visualized by staining with rhodamine-phalloidin, anti-Myo9b and anti-cortactin antibodies (B). Scale bars=10 μm. **C**, The percentage of podosome-rosette-positive macrophages. *$P<0.05$ vs. si-NS+MCP-1-untreated group; ***$P<0.001$ vs. si-NS+MCP-1 group or si-NS+MCP-1-untreated group. **D**, The macrophage migration was determined by Boyden chamber assay. *$P<0.05$ vs. si-NS+MCP-1-untreated group; ***$P<0.001$ vs. si-NS+TNF-α-untreated group or si-NS+MCP-1 group. **E**, Macrophages were transfected with si-Myo9b or si-NS for 24 h, and then infected with Ad-null or Ad-Klf5 for 24 h, podosomes were visualized as described above. Scale bars=10 μm. **F**, The percentage of podosome-rosette-positive macrophages was calculated. *$P<0.05$ vs. si-NS+Ad-null group, **$P<0.01$ vs. si-NS+Ad-null group or si-NS+Ad-Klf5 group. The data represent mean±SEM of 3 independent experiments in which 300 cells were analyzed.

# Figure 7

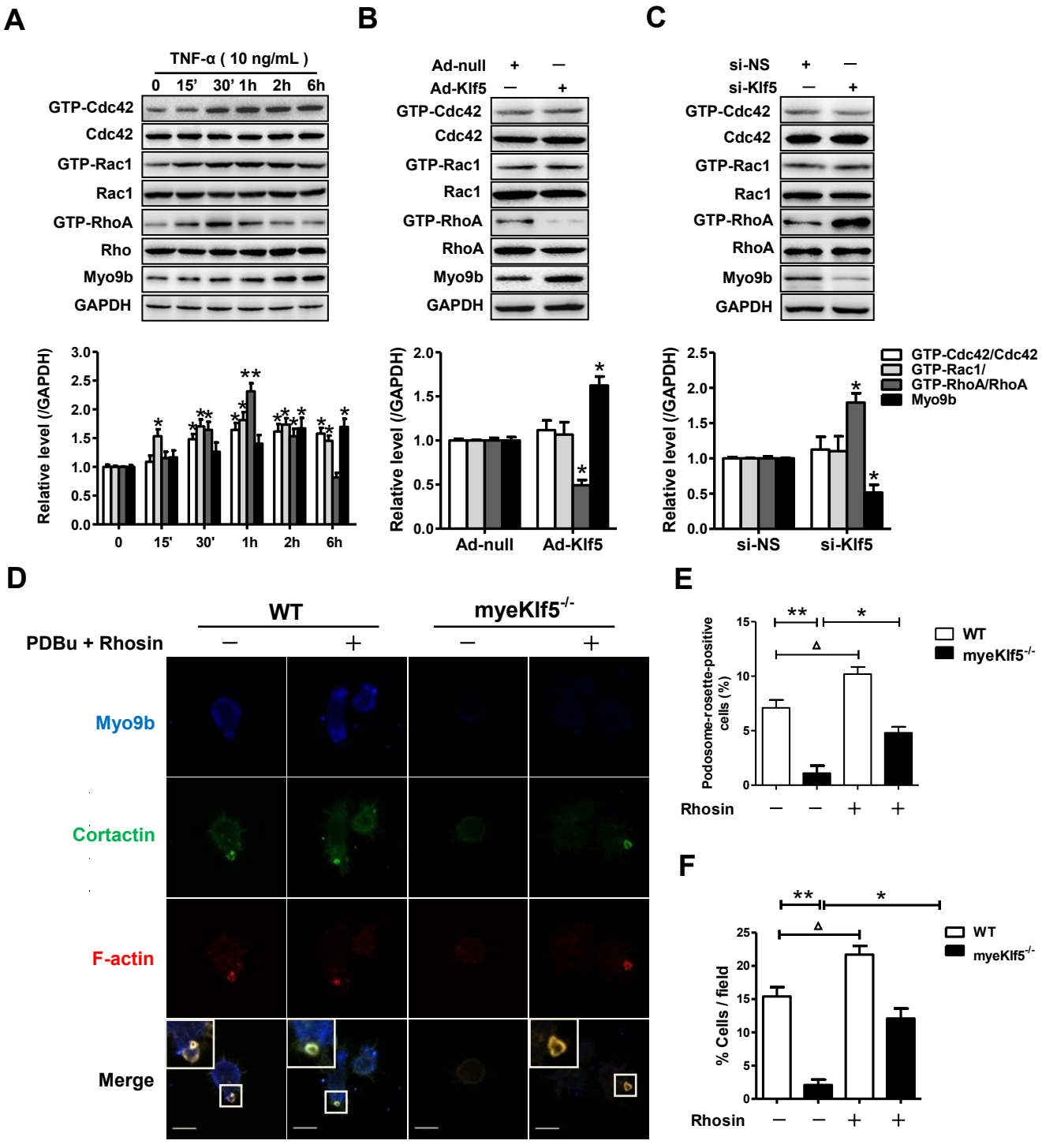
A
TNF-α ( 10 ng/mL )
0 15' 30' 1h 2h 6h
GTP-Cdc42
Cdc42
GTP-Rac1
Rac1
GTP-RhoA
Rho
Myo9b
GAPDH
Relative level (/GAPDH)
B
Ad-null + —
Ad-Klf5 — +
GTP-Cdc42
Cdc42
GTP-Rac1
Rac1
GTP-RhoA
RhoA
Myo9b
GAPDH
Relative level (/GAPDH)
Ad-null
Ad-Klf5
C
si-NS + —
si-Klf5 — +
GTP-Cdc42
Cdc42
GTP-Rac1
Rac1
GTP-RhoA
RhoA
Myo9b
GAPDH
Relative level (/GAPDH)
GTP-Cdc42/Cdc42
GTP-Rac1/
GTP-RhoA/RhoA
Myo9b
si-NS
si-Klf5
D
WT
myeKlf5-/-
PDBu + Rhosin — + — +
Myo9b
Cortactin
F-actin
Merge
E
Podosome-rosette-positive cells (%)
WT
myeKlf5-/-
Rhosin — — + +
F
% Cells / field
WT
myeKlf5-/-
Rhosin — — + +

**Figure 7. RhoA-GTP level increases after knockdown or deletion of KLF5 in macrophages. A**, Macrophages were stimulated with or without TNF-α for the indicated times. GTP-bound Cdc42, Rac1 and RhoA were determined by GST pull-down and immunoblotting with anti-RhoA, anti-Rac1 and anti-Cdc42 antibodies. Band intensities that were measured and normalized to GAPDH were shown on the below (n=3). *$P<0.05$ vs. TNF-α for 0 min. **B** and **C**, Macrophages were infected with Ad-null and Ad-Klf5 or transfected with si-NS and si-Klf5. GTP-bound Cdc42, Rac1 and RhoA were determined as described above. **D**, WT and myeKlf5$^{-/-}$ macrophages were pretreated with or without Rhosin for 2 h and then treated with PDBu for 30 min, podosomes were visualized by staining with rhodamine-phalloidin, anti-Myo9b and anti-cortactin antibodies. Scale bars=10 μm. **E**, The percentage of podosome-rosette-positive macrophages. **$P<0.01$ vs. WT + Rhosin-untreated group; *$P < 0.05$ vs. myeKlf5$^{-/-}$+Rhosin-untreated group; $^{\triangle}P < 0.05$ vs. WT+Rhosin-untreated group. **F**, The macrophage migration was determined by Boyden chamber assay. **$P<0.01$ vs. WT+Rhosin-untreated group; *$P<0.05$ vs. myeKlf5$^{-/-}$+Rhosin-untreated group; $^{\triangle}P<0.05$ vs. WT+Rhosin-untreated group. The data represent mean±SEM of 3 independent experiments in which 300 cells were analyzed.

## Figure 8

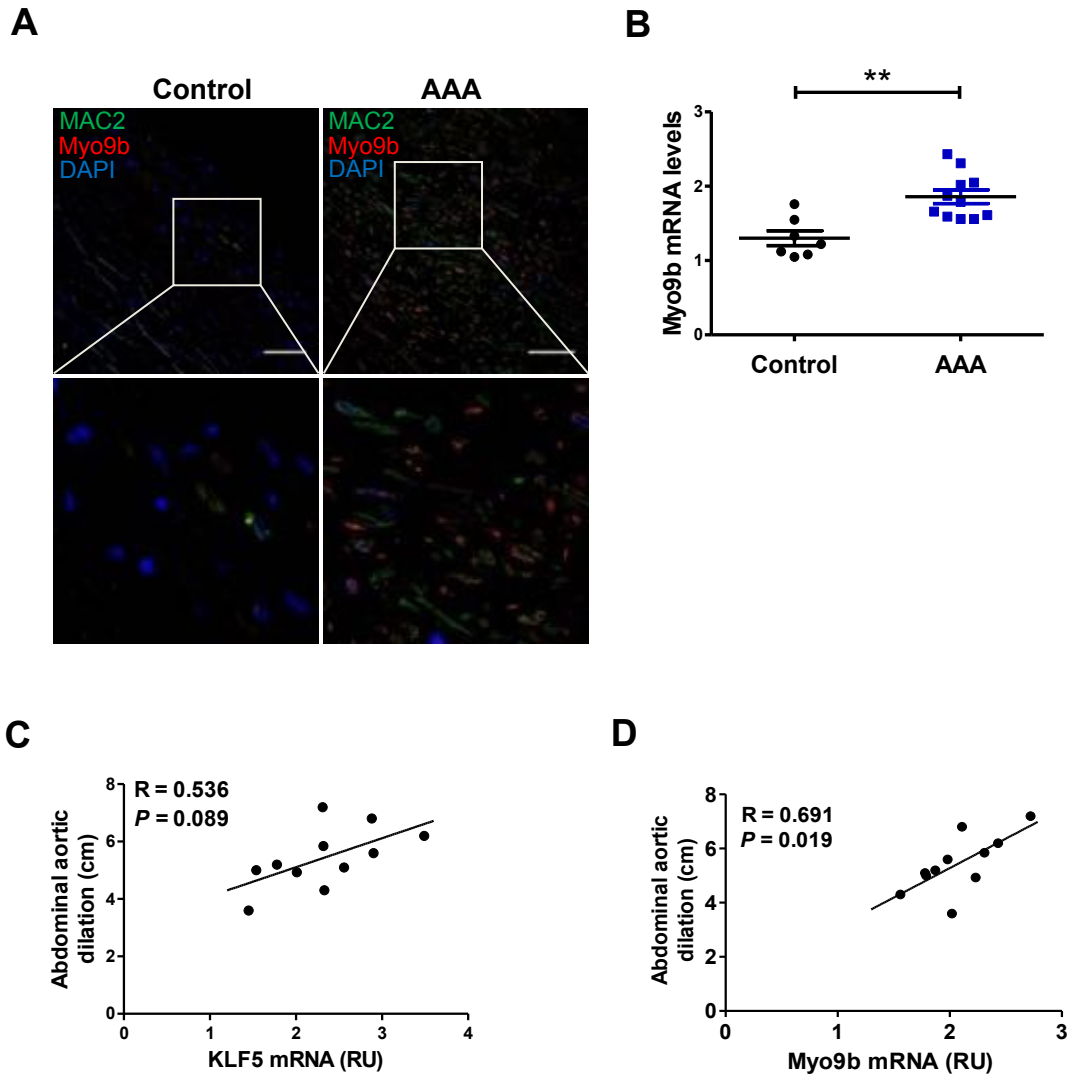


**Figure 8. Myo9b is upregulated in human AAA and is localized to macrophages.** **A**, Confocal immunohistochemistry of human AAA and non-aneurysm sections stained with MAC2, Myo9b, and DAPI. Scale bars=10 μm. **B**, Myo9b mRNA was determined by qRT-PCR in human AAA (n=11) and normal aortic tissues (n=7). **$P<$ 0.01 vs. control. **C** and **D**, Correlation analysis between KLF5 or Myo9b mRNA and human AAA size. Spearman's correlation coefficients were used to test the strength of a link between KLF5 (C) or Myo9b (D) mRNA and AAA size. Spearman's correlation coefficients and *P* values are shown in each graph. RU=relative unit.